Akash Patel[1]
Mem. ASME
Department of Mechanical Engineering,
Erik Jonsson School of Engineering and
Computer Science,
The University of Texas at Dallas,
800 West, Campbell Road,
Richardson, TX 75080
e-mails: akash.patel@arconic.com;
akash.patel@utdallas.edu

Arif Malik[2]
Mem. ASME
Department of Mechanical Engineering,
Erik Jonsson School of Engineering and
Computer Science,
The University of Texas at Dallas,
800 West, Campbell Road,
Richardson, TX 75080
e-mail: arif.malik@utdallas.edu

Ritin Mathews
Department of Mechanical Engineering,
Erik Jonsson School of Engineering and
Computer Science,
The University of Texas at Dallas,
800 W. Campbell Rd.,
Richardson, TX 75080
e-mail: ritin.mathews@utdallas.edu

Computational Method to Predict Three-Dimensional Chatter Vibration in Cold Rolling of Flat Metals

Introduced is a three-dimensional, physics-based mathematical model capable of efficiently predicting self-excited chatter vibration phenomena in the cold rolling of metal strip and sheet. The described nonlinear chatter model combines the 3D mill structural dynamics behavior with the elastic–plastic rolling process dynamics to predict conditions of instability in a single-stand 4-high mill that can lead to both third-octave and fifth-octave chatter. Formulation of the 3D chatter model is achieved by coupling the dynamic simplified-mixed finite element method with a nonlinear roll-bite process dynamics model to capture self-exciting feedback interactions. In contrast to prior approaches to model chatter in the cold rolling of flat metals, the presented method abandons several simplifying assumptions, including 1D or 2D linear lumped parameter analyses, vertical symmetry of the upper and lower halves of the roll-stack, and continuous contact between the rolls and strip. The model is demonstrated for a single-stand 4-high rolling mill considering the detrimental third-octave self-excited chatter condition. Detailed stability analyses that show time histories of the 3D mill behaviors are presented, respectively, for stable, marginally stable, and unstable rolling speeds, and for changes in the lower housing stiffness to reflect more realistic, asymmetric rolling mill conditions. [DOI: 10.1115/1.4056256]

Keywords: cold rolling, chatter, 3D mathematical model, metals, strip, machine tool dynamics, modeling and simulation, sheet and tube metal forming

Introduction

The cold rolling of metal strip or sheet is a highly coupled, dynamic process in which the structural deformation behavior of the mill (Figs. 1(*a*) and 1(*b*)) governs the rolling process parameters (Fig. 1(*c*)), and in turn, the rolling parameters govern the structural behavior. While cold rolling is generally assumed to be a quasi-static process for the purposes of mill parameter setup (e.g., for prediction/control of strip crown and flatness), small variations and disturbances that create vibrations are always present, originating from various sources such as roll eccentricity, defective gear teeth, periodic features on rolls due to grinding errors, and variations in Hertzian flattening.

As with any dynamic machine, the vibrations in a rolling mill can be free or forced, but they may also be self-excited such that sustained oscillations of increasing amplitude and energy persist even after any external disturbance vanishes. Three main vibration categories have been identified in rolling mills for which significant strip quality issues (and possibly mill damage) can arise. One type is torsional, which is forced, and arises from sources such as roll eccentricity. Torsional vibration, however, occurs at very low frequencies, typically below 30 Hz, and can be mitigated either by addressing the source or changing the rolling speed. The other two types, known respectively as "third-octave" and "fifth-octave" chatter (based on frequency ranges similar to those in musical frequency octaves), are more detrimental since they excite translational modes of the mill structure, causing periodic changes in the roll gap spacing and thus the exit gauge of the strip. Among these two, the fifth-octave type, while commonly referred to as "chatter", is nonetheless a forced vibration wherein the source typically originates in defective gear teeth, roll bearings, or drive couplings. If such disturbances excite the fifth-octave back-up roll resonance of the mill stand, then the relative motion between the work rolls and back-up rolls produces periodic roll surface defects referred to as roll chatter marks (Fig. 2). Although these chatter marks also severely affect the strip quality, the fifth-octave mode can be eliminated by addressing the source or modifying the rolling speed.

The most detrimental rolling mill vibration, not only in terms of degradation of strip quality but also because of damage to the mill structure in extreme cases, is the third-octave kind (Fig. 2), commonly referred to as "gauge chatter". The third-octave chatter is indeed a case of self-excited vibration in that any disturbance, however small, if it happens to excite a third-octave natural mode can result in a mill structural resonance caused by detrimental resonant vibration of the work rolls. This self-excitation is due to the positive feedback or "gain" originating from phase interactions between the mill stand's structural dynamics and the core rolling process variables (Fig. 1(*c*)) and leads to what is generally referred to as dynamic instability (Fig. 3). In addition to the self-excitation nature, amplitudes of vibration also rise very rapidly, and both these characteristics render third-octave chatter particularly difficult to control. Hence, it poses an ongoing problem for the rolling industry. Industrial and academic research has identified rolling speed as the most influential parameter governing its onset, yet because of the self-excited nature and origin tied to reinforcing interactions between the mill structural dynamics and the roll-bite process dynamics, the only practical way to address third-octave chatter is to reduce the rolling speed. Hence, there always exists a threshold speed for each rolling configuration (whether single stand or tandem mill), which may place major unforeseen limitations on productivity. Because of the severe consequences of third-octave chatter vibrations, significant efforts have been made to understand the general characteristics of chatter as well as to identify and predict the conditions of dynamic instability that lead to chatter.

[1]Now with Arconic Technology Center.
[2]Corresponding author.
Manuscript received May 16, 2022; final manuscript received November 11, 2022; published online December 12, 2022. Assoc. Editor: Burak Sencer.

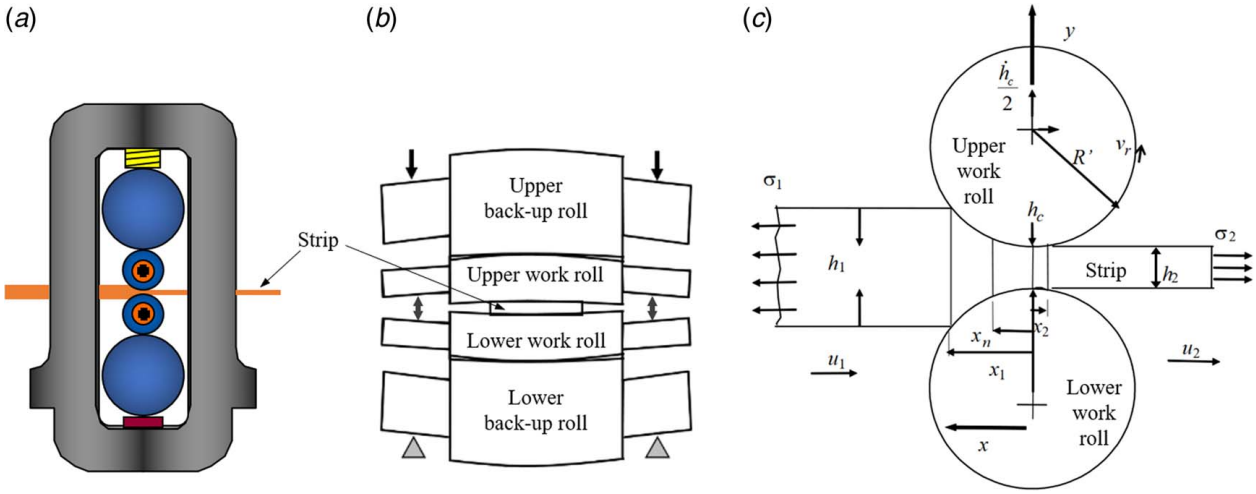

Fig. 1 Depiction of (*a*) side-view of a 4-high mill stand illustrating its various structural components, (*b*) front-view of the roll-stack showing exaggerated deformation under load, and (*c*) roll-bite geometry illustrating various rolling process parameters and positions of entry, neutral, and exit planes [1]

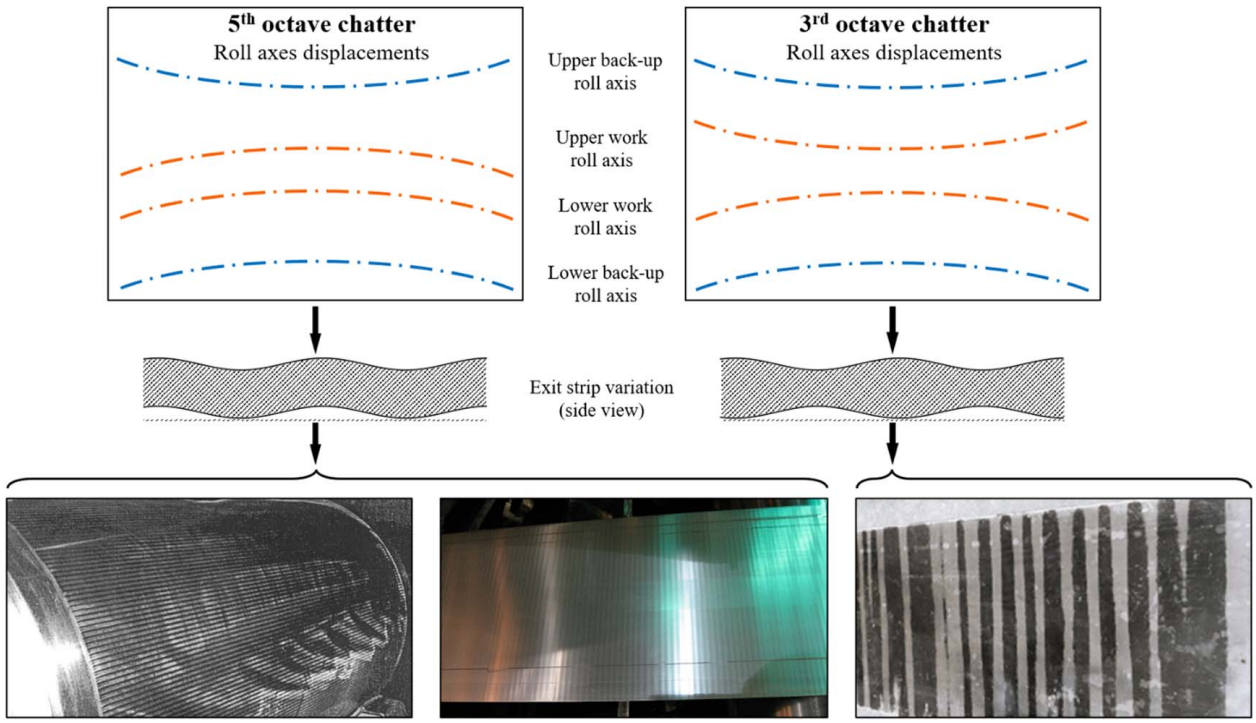

Fig. 2 In fifth-octave chatter, the work rolls (WRs) typically move together in-phase while the back-up rolls (BURs) move 180 deg out-of-phase, which results in periodic feature imprinting on the BURs due to relative roll motions (bottom left image) [2]. Also shown (bottom center image) are the fifth-octave chatter marks on the strip. In third-octave chatter, which is self-excited, the WRs and BURs each move out-of-phase while the upper and lower roll stacks move in-phase, potentially resulting in severe damage to the strip (lower right image) as well as to mill hardware [3]

Third-octave chatter is mainly attributed to the primary mechanisms of "model matching" (a term introduced in Ref. [4] when referring to negative damping effects due to coupling between the core rolling process and the mill structure in a single stand, i.e., without inter-stand tension variation effects); negative damping (where entry tension variation induces variation in force, which then acts as negative damping [5]); mode coupling (coupling of two or more principal modes of vibration as pointed out in Ref. [6]); and regenerative effects in multi-stand mills (where the variation of rolling parameters for one stand affects the other stands) [1]. For understanding the characteristics of chatter vibrations, as well as predicting their onset, attempts have been made to develop mathematical models to investigate chatter and the precursor conditions of dynamic instability. A complete chatter model necessarily involves two coupled sub-models: one to simulate/predict the rolling process phenomena (i.e., the roll-bite mechanics) and another to predict the structural dynamic behavior of the mill so that interactions between the two, as depicted in Fig. 3, can be captured and studied. The relevant major historical developments in both rolling process modeling and structural dynamics modeling for cold rolling of flat metals are briefly discussed next.

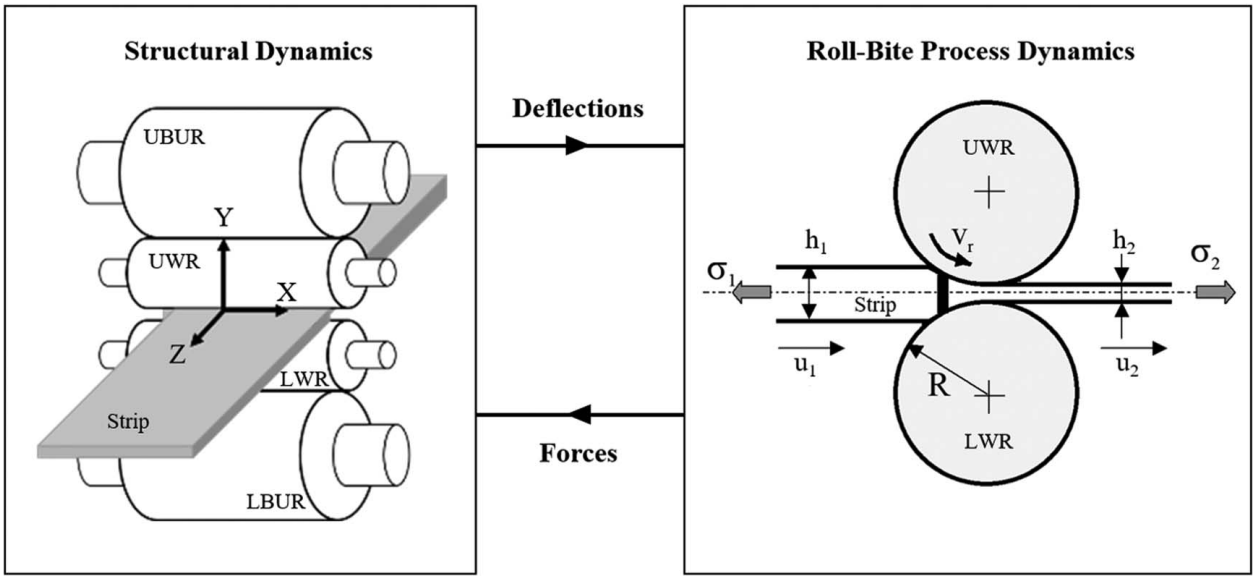

Fig. 3 Representation of the closed-loop interactions between the mill structure and rolling process parameters that can lead to self-excited chatter vibrations in the cold rolling of metals [3]

Rolling Process (Roll-Bite) Models. Historically, modeling of the rolling process itself has generally been undertaken using quasi-static conditions (thus assuming steady-state) via "slab" force analyses under 2D plane-strain conditions. However, to capture the inherent dynamics of the rolling process, the assumption that specific relationships between the various rolling parameters remain the same under dynamic conditions as for static conditions needed to be abandoned. Accordingly, Tlusty et al. [5] were among the first to put forth a complete chatter theory [7]. They attempted to show the influence of the rate of change of the roll gap on the rolling force by including the variation of exit strip thickness, which was assumed to change harmonically (according to an identically varying roll gap), while entry thickness remained constant. Although their model gave a better prediction of the rolling force variation under dynamic conditions, the formulation was still overly simplified; it was derived using the simple Tresca yield criterion, and it assumed that the neutral plane coincided with the exit plane (Fig. 1(*c*)) and also that the exit velocity remained constant and was the same as the peripheral velocity of the work rolls. Furthermore, no nonlinear effects (such as material or geometric nonlinearities) were considered.

Yun et al. [3,6,8,9] later built upon the idea of including both the change in roll gap spacing and the rate of change of roll gap spacing, while relaxing several assumptions previously employed by Tlusty. Yun et al.'s developments required a modification to the existing mass flow equation through the roll bite to accommodate the rate of change of roll gap spacing. This allowed for variation of the neutral plane location, and the resulting model was superior in predicting dynamic variations in specific rolling force. Yun et al. also argued that mode coupling between two or more principal modes of vibration could contribute to dynamic instability, and thus, they introduced the concept of a multi-directional (vertical and horizontal) model wherein motion of the work roll was allowed in more than one principal direction (as applied to the upper work roll in a symmetric 2-high mill model). However, it was Hu [4] that later proposed a more comprehensive model that could predict the dynamic force variations in both vertical and horizontal directions while relaxing yet further assumptions that an actual multi-modal, multi-directional chatter model was possible. Hu incorporated a linearized form for adaption into a state-space representation to study the stability of mills in chatter analyses.

Since then, many chatter models have used Hu's approach with varying degrees of simplification or alteration for chatter analyses, typically in the linearized form. More recently, Zhao [1] proposed an improvement by building on the idea put forth by Hu [4] of a linearized representation, but wherein Zhao included strain-hardening effects of the strip, as well as roll flattening effects neglected by Hu in Ref. [4]. Zhao also argued that the friction factor approach (introduced by Wanheim and Bay [10]) used in Ref. [4] may not be suitable for high-speed rolling where friction stress is generally significantly less than the rolled material's shear strength. Zhao's formulation for the prediction of rolling force is based on the original Bland and Ford equation [11].

Mill Structural Models. In the context of chatter investigations, structural dynamics modeling has not received as much attention as roll-bite modeling. Indeed, all but a few chatter models in the published literature exclusively use linear lumped parameter systems (either uni-modal [5,7,12–16] or multi-modal [6,8,9,17–23]) in which the mill stand is represented by a simple spring-mass-dashpot system. A few attempts have been made to include a 3D roll-stack modeling approach to emulate the mill structural dynamics [24–27], although not for any chatter investigation. Implementation of structural models over the years for general dynamic analyses, including characteristics and drawbacks, were discussed in detail in recent work by the authors in Ref. [27] in which an efficient, general-purpose, nonlinear 3D dynamic model was introduced to predict the time history of structural dynamics for various mill configurations. As detailed later, this structural model in Ref. [27] is adapted for the chatter analyses in the work here because it addresses some of the major research deficits in prior chatter investigations, specifically:

- Lack of the 3D bulk-body deformation behavior (i.e., no accommodation for transverse bending, non-uniform Hertzian roll flattening, or shear-type roll-stack deformations) due to the adoption of linear, lumped parameter systems.
- Assumption of vertical symmetry of the mill about the strip thickness mid-plane.
- Assumption of constant and continuous contact between the strip and the work rolls.
- Representation of nonlinear contact behaviors using discrete, linear springs (including for "hard" nonlinearities such as localized loss of work-roll/strip contact at transverse locations across the strip width, and "soft" nonlinearities such as varying Hertzian contact flattening stiffness).
- Inability to adapt to different mill configurations, particularly complex 20-high cluster mills.

- Inflexibility to account for transverse variations in contact conditions based on the presence of conventional flatness control mechanisms, as well as the inability to capture micro-scale to macro-scale transverse contact mechanics coupling behaviors [28].

As shown in Ref. [27], abandoning the assumptions above provides for improved physics-based predictions of mill structural behavior, which can include efficient time histories of the strip thickness profiles (due to capturing of the 3D bulk-body deformations), as well as coupled mode shapes of the rolls (e.g., coupling of bending and non-uniform Hertzian flattening). Accordingly, introduced and demonstrated in this work is an n-degree-of-freedom (n-DOF), nonlinear, 3D chatter model obtained by coupling the dynamic simplified-mixed finite element method structural model (D-SM-FEM) [27] with the roll-bite model described by Zhao in Ref. [1]. While the approach presented is readily adaptable to multi-stand (tandem) mills, the stability analyses in this work are demonstrated on single-stand mill configurations to allow for a sufficiently detailed study of the associated chatter phenomena, which include new observations based on the relaxation of assumptions mentioned earlier.

Mathematical Model

Described next is a brief mathematical description of the dynamic structural model (D-SM-FEM) and its coupling with the roll-bite process model. The resulting consolidated 3D model is capable of thorough chatter investigations, including the most detrimental third-octave self-excited mode that drives ongoing research because of its severe limitations to rolling mill speed and mill productivity. A detailed description of the D-SM-FEM structural model formulation is given by the authors in the previous work; however, key equations are reiterated below.

Structural Dynamics Model. The 3D dynamic roll-stack deformation structural model or D-SM-FEM, detailed in Ref. [27], involves combining the static simplified-mixed finite element model (SM-FEM) [29,30] with a Nemark Beta direct time integration technique (NM-Beta). Although full details of the SM-FEM model are not included here, the key equations are given in Eqs. (1*a*)–(1*c*), wherein the 3D displacement vector of translations and rotations with respect to the local (x, y, z) coordinate frame at each node j is $\boldsymbol{u}_j = \{u_j\ v_j\ w_j\ \theta_{xj}\ \theta_{yj}\ \theta_{zj}\}^T$. The 4-high mill schematic in Figs. 4(*a*) and 4(*b*) provides for visual interpretation. Terms $[\boldsymbol{K}_T^{1,i}]$ and $[\boldsymbol{K}_T^{2,i}]$ in Eq. (1*b*) are 12×12 Timoshenko elements of adjacent contacting rolls, 1 and 2, such as the work roll and back-up roll (the strip is assigned zero bending/shear stiffness). The second term on the right side of Eq. (1*b*) contains continuous foundation stiffness coupling terms between the two adjacent bodies. Parameter θ in Eq. (1*c*) is the inter-roll inclination angle, which accounts for both vertical and cluster roll-stack configurations ($\theta = 90$ deg for vertically oriented 2-high, 4-high, and 6-high mills [27])

$$[\boldsymbol{K}_G(\boldsymbol{u})]\,\boldsymbol{u} = \boldsymbol{f}(\boldsymbol{u}) \tag{1a}$$

$$[\boldsymbol{K}_G^{1,2,i}] = \begin{bmatrix} [\boldsymbol{K}_T^{1,i}] & [0] \\ [0] & [\boldsymbol{K}_T^{2,i}] \end{bmatrix} + \begin{bmatrix} \int_0^{l_i} k_{f_{eq}}(x)[\boldsymbol{N}_{11}]dx & -\int_0^{l_i} k_{f_{eq}}(x)[\boldsymbol{N}_{12}]dx \\ -\int_0^{l_i} k_{f_{eq}}(x)[\boldsymbol{N}_{21}]dx & \int_0^{l_i} k_{f_{eq}}(x)[\boldsymbol{N}_{22}]dx \end{bmatrix} \tag{1b}$$

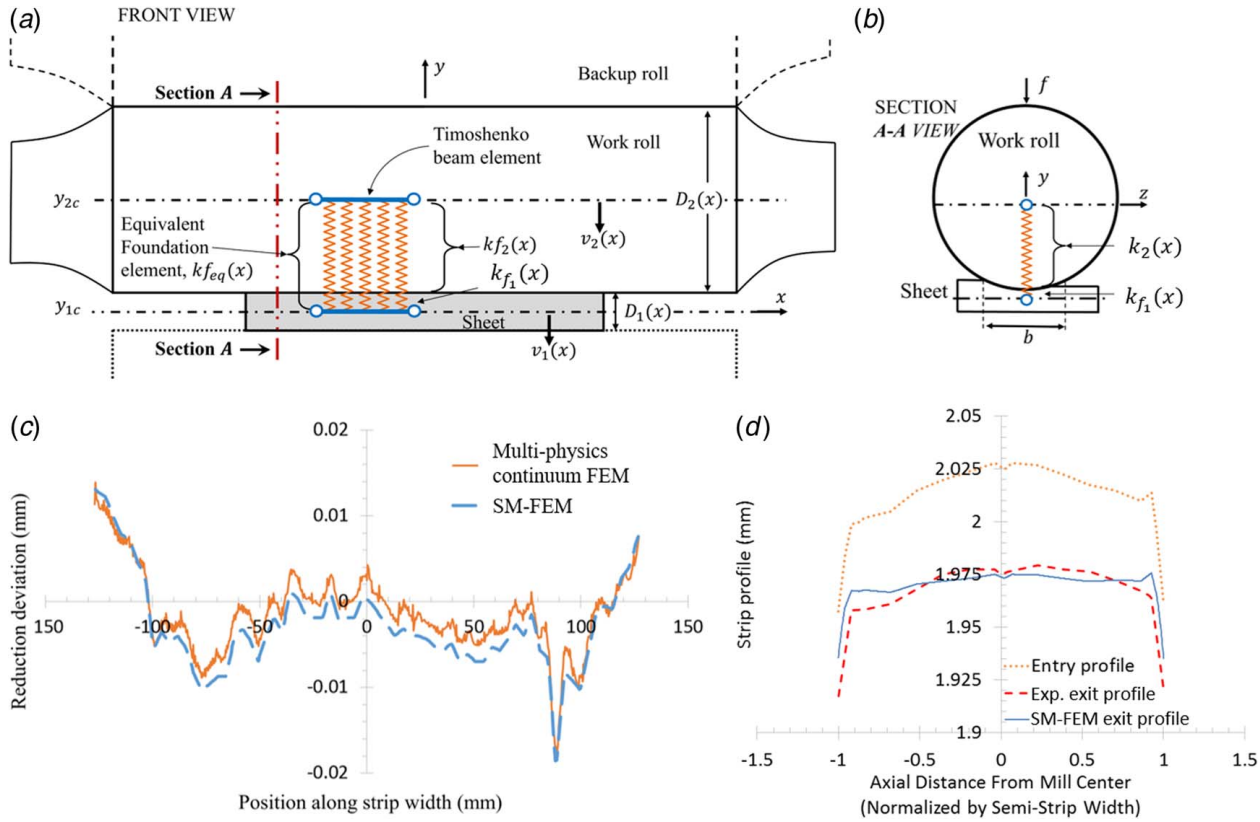

Fig. 4 (*a*) and (*b*) Schematic of static simplified-mixed finite element method (SM-FEM) on the upper section of the 4-high mill [29,30]. (*c*) Comparison of strip reduction deviation between SM-FEM and a multi-physics continuum finite element model (using Abaqus® v6.14) for experimentally measured work-roll dia. profiles [31,32]. (*d*) Comparison between SM-FEM predicted strip exit thickness profile and measured thickness profile from a 6-high continuously variable crown (CVC) mill [30,33]

Each integrand term $[N_{pq}]$ in Eq. (1*b*), for $p, q \in \{1, 2\}$, is defined as follows:

$$[N_{pq}] = [N_{vp}]^T [N_{vq}] \sin^2\theta + [N_{wp}]^T [N_{wq}] \cos^2\theta + [N_{vp}]^T [N_{wq}] \sin\theta\cos\theta + [N_{wp}]^T [N_{vq}] \sin\theta\cos\theta \quad (1c)$$

Figures 4(*c*) and 4(*d*) show, respectively, multi-physics and experimental comparisons for the SM-FEM model prediction capability. Figure 4(*c*) indicates close agreement in the strip reduction deviation between SM-FEM and a large-scale, multi-physics continuum finite element model (Abaqus® v6.14) [31]. Figure 4(*d*) shows agreement between the SM-FEM predicted exit strip thickness profile and the corresponding experimentally measured profile from a 6-high continuously variable crown (CVC) mill [30,32]. Given these favorable comparisons, the SM-FEM model is assumed appropriate for chatter model adaption. Moreover, as detailed in Ref. [27], the damped steady-state solution using the dynamic version of the SM-FEM model matches the original static solution, demonstrating spatiotemporal convergence and numerical stability.

Integration of the above-mentioned static global system of equations in the time domain is achieved via NM-Beta using average acceleration method parameters ($\gamma = 0.5$ and $\beta = 0.25$). The corresponding global, discretized equations of motion using the static SM-FEM model can be written as

$$[\boldsymbol{M}]\ddot{\boldsymbol{u}} + [\boldsymbol{C}]\dot{\boldsymbol{u}} + [\boldsymbol{K}_G(\boldsymbol{u})]\boldsymbol{u} = \boldsymbol{f}(\boldsymbol{u}, t) \quad (2)$$

where $\boldsymbol{u}$ is the displacement vector, $[\boldsymbol{M}]$ is the mass matrix, $[\boldsymbol{K}_G(\boldsymbol{u})]$ and $\boldsymbol{f}(\boldsymbol{u}, t)$ are the stiffness matrix and load vector from the SM-FEM formulation given earlier. One of the advantages of the NM-Beta method is that even though it is an implicit time integration method, it is still possible to obtain explicit expressions based on the previously known solutions as the time is incrementally advanced. With known initial conditions, the displacement vector can be obtained per Eq. (3)

$$[\hat{\boldsymbol{K}}]\boldsymbol{u}(t + \Delta t) = \hat{\boldsymbol{F}}(t + \Delta t) \quad (3)$$

where $[\hat{\boldsymbol{K}}]$ and $\hat{\boldsymbol{F}}$ are the effective stiffness matrix and effective load vector, respectively, defined by Eqs. (4*a*) and (4*b*)

$$[\hat{\boldsymbol{K}}] = [\boldsymbol{K}] + \left(\frac{1}{\beta\Delta t^2}\right)[\boldsymbol{M}] + \left(\frac{\gamma}{\beta\Delta t}\right)[\boldsymbol{C}] \quad (4a)$$

$$\hat{\boldsymbol{F}}(t + \Delta t) = \boldsymbol{f}(t + \Delta t) + [\boldsymbol{M}]\left[\frac{1}{\beta\Delta t^2}\boldsymbol{u}(t) + \frac{1}{\beta\Delta t}\dot{\boldsymbol{u}}(t) + \frac{(1 - 2\beta)}{2\beta}\ddot{\boldsymbol{u}}(t)\right] + [\boldsymbol{C}]\left[\frac{\gamma}{\beta\Delta t}\boldsymbol{u}(t) - \frac{(\beta - \gamma)}{\beta}\dot{\boldsymbol{u}}(t) - \frac{(2\beta - \gamma)\Delta t}{2\beta}\ddot{\boldsymbol{u}}(t)\right] \quad (4b)$$

With known displacement vector for the current time-step, acceleration and velocity can then be obtained for the current time per Eqs. (5) and (6)

$$\ddot{\boldsymbol{u}}(t + \Delta t) = \frac{\boldsymbol{u}(t + \Delta t) - \boldsymbol{u}(t)}{\beta\Delta t^2} - \frac{\dot{\boldsymbol{u}}(t)}{\beta\Delta t} - \ddot{\boldsymbol{u}}(t)\left(\frac{1}{2\beta} - 1\right) \quad (5)$$

$$\dot{\boldsymbol{u}}(t + \Delta t) = \frac{\gamma(\boldsymbol{u}(t + \Delta t) - \boldsymbol{u}(t))}{\beta\Delta t} + \dot{\boldsymbol{u}}(t)\left(1 - \frac{\gamma}{\beta}\right) + \Delta t\, \ddot{\boldsymbol{u}}(t)\left(1 - \frac{\gamma}{2\beta}\right) \quad (6)$$

In this D-SM-FEM formulation, the use of a "dynamic strip modulus" (Fig. 5) effectively makes the system behave elastically (i.e., linearly) at each time-step rather than being nonlinear elastic–plastic in time. Moreover, since both the "hard" nonlinearities (e.g., loss of contact) and "soft" elastic–plastic-type nonlinearities are accounted for iteratively *within* each time-step (i.e., inside the SM-FEM per Eq. (1)), the system is piecewise linear in the time domain. In such a piecewise linear system, classical damping (i.e., mass and initial stiffness proportional damping) can be applied without the concern of any spurious damping issues. The mill housing stiffness is included via discrete spring representation, as in Fig. 6.

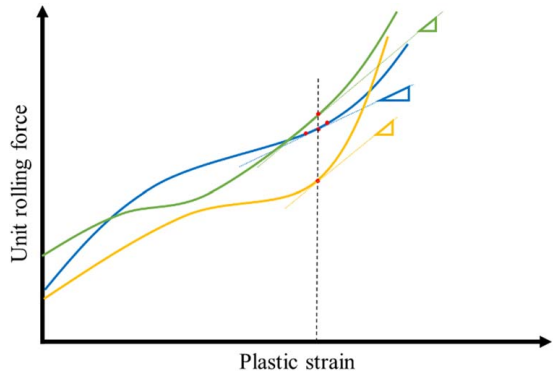

Fig. 5 Depiction of "dynamic strip modulus" as the tangent (or secant) of the unit rolling force versus plastic thickness strain (reduction) at the working point of the mill. The strip modulus can change with variations in the thickness strain on the same unit force versus plastic strain curve (shown as three dots on same curve) such as in the case of model matching phenomena (introduced by Hu [4]) where speed, tensions, etc., remain constant while the required rolling force effectively becomes a function only of the roll gap and rate of change of roll gap. The strip modulus can also vary based on an entirely new force versus plastic strain relationship (even for the same thickness strain) due to variation in the tensions and speed, as shown with distinct curves.

Roll-Bite Process Model. A critical aspect in replicating dynamic interactions between the rolling process and the mill structural dynamics relates to real-time variations in the working point or "operating point" relations between specific rolling force and plastic strain of the rolled strip, which change according to perturbations the roll gap, entry/exit plane locations, speeds, and tensions. As mentioned earlier and illustrated in Fig. 5, these variations in the working point are incorporated in the D-SM-FEM via the concept of a *dynamic* strip modulus (*SM*) based on the secant (or tangent) relationship between specific rolling force and plastic strain at the working point, but where the strip modulus is updated at every time-step per Eq. (7)

$$SM = k_{f_1} = \frac{f}{h_1 - h_2} \quad (7)$$

where h_1 and h_2 represent the entry thickness and the (anticipated) exit thickness at the widthwise center location of the strip, and f is the specific rolling force required to achieve the thickness reduction, $h_1 - h_2$.

As discussed in the earlier Structural Dynamics Model section, numerous dynamic rolling process models have been developed over the years with varying degrees of assumptions and simplifications, and each can be used to obtain the required rolling (separation) force exerted by the strip at the given time-step. As noted already, the homogeneous dynamic rolling process model by Zhao [1] is used. The corresponding input and output parameters, along with their relationships, are reiterated below.

Referring again to Fig. 1(*c*), the input parameters include the current roll gap and the rate of change of roll gap (h_c, $\dot{h}_c$), the strip entry thickness (h_1), the tensile stress/tension at entry and exit sides (σ_1, σ_2), and the peripheral velocity of the roll (v_r). Output parameters include the specific rolling force (f) and the strip velocities at the entry and exit (u_1 and u_2). The relationship between the input and output parameters of the roll-bite model is given in Eqs. (8)–(10). Note that the model also gives total

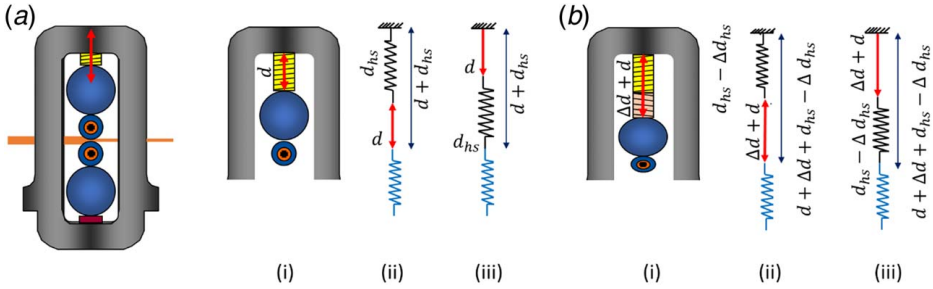

Fig. 6 Illustration of loading condition and model implementation considering mill housing stiffness displacement (d_{hs}). Depicted are upper sections of a mill housing in (*a*) initial (unloaded) position and (*b*) loaded position. Also shown in (*a*) and (*b*) are (*i*) the mill posts, (ii) the equivalent discrete housing stiffness representation via springs, and (iii) alternate equivalent stiffness representation that replicates the hydraulic cylinder movement *d* in (ii), even in the loaded position (reproduced from Patel et al. [27]). Note that in Ref. [27] the housing stiffness was implemented only on the top stack whereas ends of the lower back-up roll (bearing locations) were numerically fixed to represent rigid (infinite stiffness) lower housing supports. In this work, however, finite housing stiffness is employed at both upper and lower mill housing supports.

torque, M as an output, although it is not needed in the current work.

$$f = \int_{x_n}^{x_1} p^- dx + \int_{x_2}^{x_n} p^+ dx \tag{8}$$

$$u_1 = \frac{1}{h_1}\left[v_r\left(h_c + \frac{x_n^2}{R'}\right) + (x_1 - x_n)\dot{h}_c\right] \tag{9}$$

$$u_2 = \frac{u_1 h_1 + (x_2 - x_1)\dot{h}_c}{h_c + \frac{x_2^2}{R'}} \tag{10}$$

In Eqs. (9) and (10), R' is the deformed work-roll radius (calculated per Eq. (11)), and p^- and p^+ are the entry side and exit side pressures, respectively, as per Eqs. (12) and (13)

$$R' = R\left[1 + \frac{16(1-\nu)^2}{\pi E}\frac{f}{(h_1 - h_2)}\right] \tag{11}$$

$$p^- = (K_{f,1} - \sigma_1)\frac{K_f h}{K_{f,1} h_1} e^{\mu(H_1 - H)} \tag{12}$$

$$p^+ = (K_{f,2} - \sigma_2)\frac{K_f h}{K_{f,2} h_2} e^{\mu(H - H_2)} \tag{13}$$

$$H = 2\sqrt{\frac{R'}{h_c}}\tan^{-1}\left(\frac{x}{\sqrt{R' h_c}}\right) \tag{14}$$

$$K_f = s_0 + A\varepsilon^n \tag{15}$$

In the above-mentioned formulation, K_f is the deformation resistance of the strip, s_0 is the yield strength, and A and n are the respective strain-hardening parameters of the strip material. Longitudinal positions of the entry plane (x_1), neutral plane (x_n), exit plane (x_2), and strip thickness at position x relative to the centerline between the work rolls are required in the above and can be obtained through the following relations:

$$x_1 = \sqrt{R'(h_1 - h_c)} \tag{16}$$

$$x_2 = \frac{R' h_c \dot{h}_c}{2\left[u_1 h_1 - x_1 \dot{h}_c\right]} \tag{17}$$

$$x_n = \sqrt{R' h_c}\tan\left\{\frac{1}{4}\sqrt{\frac{h_c}{R'}}\left(H_1 + H_2 - \frac{1}{\mu}\left[\frac{K_{f,2} - \sigma_2}{K_{f,1} - \sigma_1}\frac{h_1 K_{f,1}}{h_2 K_{f,2}}\right]\right)\right\} \tag{18}$$

$$h = h_c + \frac{x^2}{R'} \tag{19}$$

In Zhao's original work, the above-described roll-bite model was used following linearization due to its nonlinear and implicit nature. In this work, however, the equations are used in their original nonlinear form, as is in Eqs. (12)–(19). Once the entry, neutral, and exit positions are computed (iteratively) and the neutral point location converges (to within 0.1%), the entry side pressure, p^-, and exit side pressure, p^+, are integrated to obtain the specific rolling force, which is then used to update the dynamic strip modulus in Eq. (7). Since the roll-bite model only requires the roll gap (h_c) and rate of change of roll gap ($\dot{h}_c$), the specific force can be obtained iteratively from the roll-bite model until convergence; it is then directly incorporated into the structural dynamics model via the dynamic strip modulus. The advantage is emphasized that all hard and soft nonlinearities arising from structural and contact behaviors are handled within the D-SM-FEM model itself, so there is no need for linearization of the roll-bite model relationships unless an increase in computational efficiency is sought (which may not be justifiable considering the accuracy improvement in the results and retained efficiency even when employing the nonlinear relations).

Single-Stand Chatter Model. Implementing the coupling between the D-SM-FEM structural model and the roll-bite model via the dynamic strip modulus concept, a single-stand chatter model can be formulated, as shown schematically in Fig 6.

Here, the inter-stand tension effects are incorporated by including entry and exit side winder/unwinder mandrels. The instantaneous variations in tensile stress/tension at the entry and exit are computed per Hooke's law (Eqs. (20) and (21))

$$\sigma_{j,t} = \sigma_{j,t-\Delta t} + \Delta\sigma_j \tag{20}$$

$$= \sigma_{j,t-\Delta t} \pm E/L\int_{t-\Delta t}^{t} (\Delta u_j - \Delta u_{m_j})dt \tag{21}$$

where $j \in [1, 2]$ for entry side and exit side, respectively, and u_m represents the mandrel velocity. For simplicity, it is assumed that mandrel velocities are constant, i.e., $\Delta u_{m_1} = \Delta u_{m_2} = 0$.

Table 1 Material constitutive model (isotropic hardening) parameters of 301 stainless steel strip

Material	Yield strength (MPa)	Strength coefficient (MPa)	Strain-hardening exponent
Stainless steel 301	283	2987.49	0.7475

Table 2 4-high mill dimensions and rolling parameters

Parameter	Value
Work-roll diameter	76.2 mm
Back-up roll diameter	304.8 mm
Work roll face length	305 mm
Back-up roll face length	305 mm
Work-roll neck diameter	50.8 mm
Back-up roll neck diameter	187.2 mm
Work roll neck length	152 mm
Back-up roll neck length	152 mm
Distance between bearings on work roll	457 mm
Distance between bearings on back-up roll	457 mm
Work roll and back-up roll Young's modulus	207 GPa
Strip width	209.6 mm
Entry thickness	2.576 mm
Exit thickness	2.382 mm
Reduction ratio	7.495%
Strip modulus (initial)	10.14 GPa

Results and Discussion

The goal accompanying the case studies presented in this section is to demonstrate the ability of the combined D-SM-FEM method and the adopted roll-bite force model to address the absence of chatter models in literature employing 3D bulk-body deformation effects and to address the limitations identified earlier regarding structural modeling deficits in the existing chatter models. Also, while the types of case studies and stability analyses typically found in the literature, e.g., studying the effects of friction, tension variations, etc., are possible to examine, the aim of the cases presented here is instead to demonstrate the 3D chatter modeling capability while also rigorously accounting for the nonlinear roll-bite coupling behavior and the nonlinear structural dynamics/bulk-body deformation effects.

4-High Mill With Symmetric Housing Stiffness. Analogous to most prior chatter studies in which a vertical symmetry assumption is employed, the cases involving a 4-high mill in this section employ identical mill housing stiffness at the top and bottom support regions (Fig. 5) to replicate symmetric conditions (asymmetric housing stiffness cases are presented in the next section). Three studies are provided, corresponding respectively to stable, marginal, and unstable cases, demonstrating the ability of the 3D chatter model to predict self-excited vibrations.

The D-SM-FEM structural dynamics model is initially executed without coupling the roll-bite process model until a steady-state is reached (this part of the simulation, including spatial and temporal discretization, is the same as that presented in the previous work to investigate only the structural dynamics [27], where the strip and mill data and rolling conditions are listed in Tables 1 and 2. However, note that housing stiffness is applied to both upper and lower BUR supports, versus only at the upper support in Ref. [27]). Steady-state is defined in this context as the relative displacement of upper work roll (UWR) converging to within 10^{-4}%, or an absolute value of 10^{-8} m after the mill is loaded with instantaneous displacement boundary condition at the top of the housing spring element, as shown in the earlier Fig. 6.

For convenience, it is assumed based on prior verification that steady-state is attained after 250 ms (which corresponds to the 5000th time-step in a temporal convergence study with the same mill and conditions as in Ref. [27]). Once the steady-state is reached, the roll-bite model is coupled with the structural dynamics model and the dynamic strip modulus becomes active in each time-step according to the specific force computed via the roll-bite model. Note that damping in the system is simultaneously reduced to 2.5% of the critical damping instead of the previous 12% used to attain steady-state.

Even though at this 250 ms time instant, the system can be viewed for practical purposes as at steady-state (since roll gap changes are on the order of 10^{-11} m), note that with such a nonlinear dynamic system, "true" steady-state is impractical to achieve; this is because residual vibrations manifested by these very slight changes in the roll gap are still present, and may in fact be reflective of actual vibrations in the mill due to cyclic elastic Hertzian flattening of the rolls, or other sources that are always present in any real rolling operation (even absent any variations in the roll speeds or entry thickness of the strip). As such, in the following results discussed, note that all variation onsets in the rolling force and other parameters are simply due to changes in the roll gap that originate from these very small residual vibrations. In other words, there is no external disturbance used to excite the system. Also note that the magnitudes of steady-state parameters of the roll-bite process model and their variations in the transient state are functions of many other parameters, including the reduction ratio, friction conditions, and material behavior considering strain-hardening, etc. Absent comprehensive experimental data with which to compare and validate the results, the parameters in these simulations are in a sense arbitrary, but are selected based on practical knowledge and experience of the rolling process. This latter point is understood

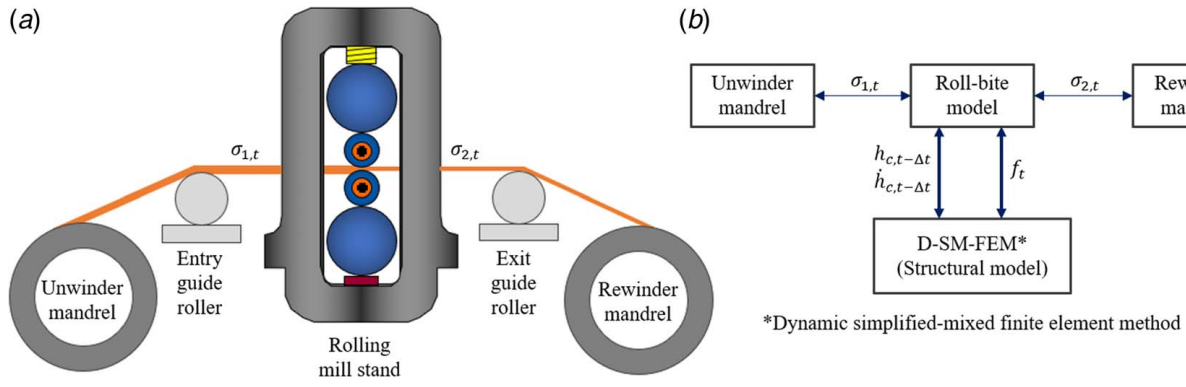

Fig. 7 Schematic illustration of single-stand chatter model, obtained by coupling of the structural model (D-SM-FEM) and roll-bite model, and showing relay of coupling parameters, including the roll gap spacing (h_c), rate of change of roll gap spacing ($\dot{h}_c$), and roll separation force (the force is subsequently used to update the dynamic strip modulus)

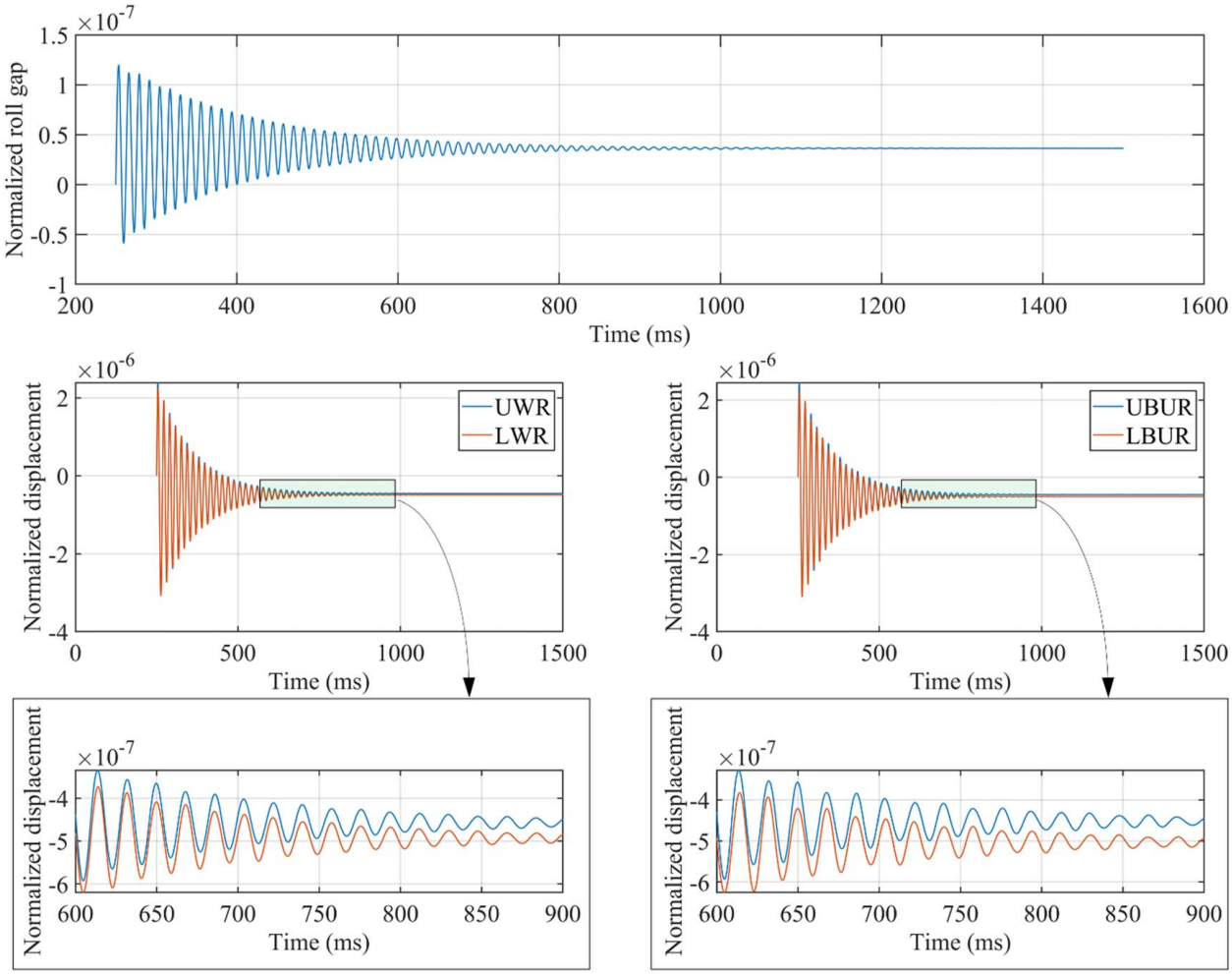

Fig. 8 Time history of (top) normalized roll gap at the axis center; (bottom left) normalized displacement of upper and lower work roll mid-points, and (bottom right) normalized displacement of upper and lower back-up roll mid-points for stable case (v_r = 5.08 m/s) with symmetric housing stiffness

given that complete data corresponding to 3D chatter studies are non-existent in the published literature.

Stable Case. Figure 8 shows the variation in the roll gap (at the mill center with respect to the widthwise direction of the strip) as well as the displacements of UWR, lower work roll (LWR), and back-up rolls (UBUR, LBUR) for a rolling speed of 5.08 m/s. Here, note that for the new steady-state conditions after coupling (at 1400 ms in these plots), the roll gap variation (and thus roll displacements) do not revert to the relative zero with respect to the imposition of roll-bite coupling at 250 ms. In other words, the roll gap seems at first to be permanently changed; however, this is not the case. It is because the assumed steady-state reference with respect to which the results are plotted (i.e., those at 250 ms) is not actually the true steady-state. Recall that even at 250 ms the rolls were still vibrating with displacements on the order of 10^{-9} m and were still progressing toward the true steady-state. Hence, it is due to this specific initial condition displacement at the moment of coupling that we see an apparently different steady-state in this stable system. Also, note that the phase difference between the upper and lower halves of the roll stack, i.e., between the UWR and LWR and between the UBUR and LBUR, is zero so both upper and lower roll stacks are in-phase. Before the roll-bite model coupling, when the mill was loaded, there existed a continuously changing non-zero phase difference due to the initial instantaneous loading condition and damping, however, with progressing time the phase difference was converging toward zero (as the system converged toward steady-state). In a stable system like this, this trend is maintained even after coupling with the roll-bite model occurs. In fact, the trend is accelerated such that the upper and lower stacks quickly go in-phase. The reason for this accelerated convergence to zero phase difference is that, before the coupling, only structural damping (provided via Rayleigh damping) played a role in the system stability or removing energy from the system, whereas after the coupling, in addition to the structural damping the positive damping from the variations in the roll-bite parameters also begins removing energy from the system.

Moreover, as is widely known, structural damping is proportional to velocity, so as the system converges to steady-state, the amount of energy removed by structural damping also converges to zero. Accordingly, the rate of convergence towards the true steady-state also continues to decline (hence, the reason why steady-state needs to be defined using convergence criteria for such a nonlinear system). On the other hand, after coupling, the energy removed as a result of the phase difference between the various rolling parameters assists the system as a whole to attain a steady-state more rapidly.

It is worth mentioning here that one of the assumptions in Zhao's roll-bite model is that the product of strip thickness and deformation resistance of the strip along the contact arc remains constant. This is a fair assumption for significantly hardened strips typically entering the latter stands in a tandem mill, but it may be inappropriate for annealed strips entering the first stand. Notwithstanding this simplification, the objective of this work is on the development of a 3D chatter model with the sufficient predictive capability to identify dynamic instabilities; more suitable roll-bite model representations

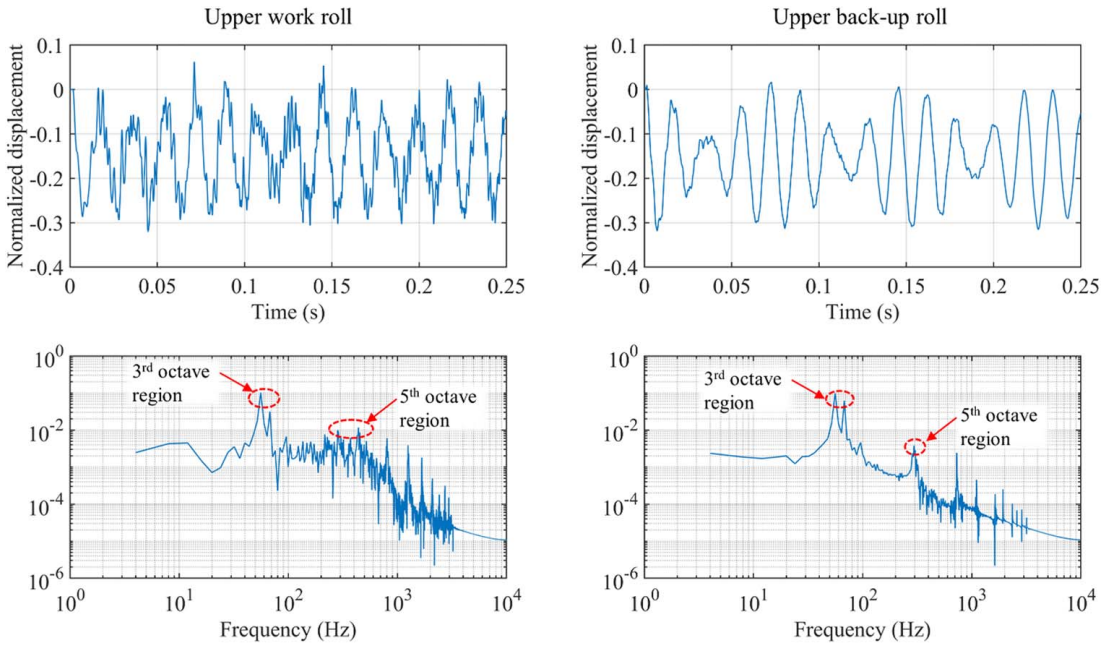

Fig. 9 Time history of displacement of mid-point of (top left) upper work roll and (top right) upper back-up roll. Also shown are the corresponding frequency response plots showing the third-octave and fifth-octave frequency regions. Note that these results are for the undamped system that is also not coupled to the roll-bite process model, i.e., the 3D structural model only.

corresponding to the actual mill and strip conditions with which this new modeling approach is applied can be readily incorporated.

Figure 9 shows the displacements of the UWR (top left) and UBUR (top right) with corresponding frequency responses shown below for the undamped system (i.e., not coupled to the roll-bite model). Various natural frequencies of the mill structure components (UWR and UBUR) falling within the third- and fifth-octave ranges are clearly seen. Note that since this dynamic behavior is governed solely by the uncoupled D-SM-FEM model, the frequency responses shown are for the mill structural components and the strip modulus corresponding to the required rolling force at the start of the simulation. Once coupling occurs, the frequency responses change continuously due to the implementation of the dynamic strip modulus (the foundation stiffness representing the strip is changed). Therefore, note that even though such plots of frequency response can be generated for estimation of the natural third-octave and fifth-octave chatter frequencies, doing so is not as effective in a nonlinear system as it is in a linear system since the stiffness is changing at every time-step. Indeed, for a change in rolling speed, a new frequency response will be generated. Also note that, due to structural damping, many frequencies will be suppressed to a great extent in a damped case or stable case, thus not revealing significant power in the frequency response plot although these could in fact be excited and become resonant if the mill is simulated (operated) at that speed. 3D Plots showing the time history of the true mode shapes of the rolls for the stable case are in Appendix Figs. 18 and 19.

Marginally Stable Case. As one would expect from industrial/experimental observations, with an increase in speed the system generally tends toward an unstable system because rolling speed is identified as the most influential parameter governing the frequency of mill structure component vibrations. In the transition from a stable to unstable speed, there exists usually some speed (known as the critical or threshold speed) that represents the limit of stability wherein the system is marginally stable, and thus, increasing the speed beyond this point will result in an unstable system (until any subsequent stable region is reached).

Figure 10 demonstrates the results of a marginally stable case for this mill configuration obtained at a rolling speed 8.84 m/s. Note that, being marginally stable, the variation in the roll gap (or structural vibration) would persist indefinitely regardless of amplitude; note that this amplitude of the sustained vibration depends on the energy balance between the energy added by negative damping effects via the roll-bite model and the energy removed by the structural damping (structural damping here represents both the mill structure damping and material damping arising due to plastic deformation of the strip).

Because of the interactions between roll-bite parameter variations and the structural model, there is a phase difference between the upper and lower roll-stack portions of the mill. Moreover, since the variation in the specific force affects the dynamic strip modulus, i.e., the instantaneous foundation stiffness of the strip, any change in this stiffness is experienced by the upper and lower stack portions in opposite directions. Note that if the rolling speed were sufficiently low for the system to be stable (such that the negative damping effects from the roll-bite model do not dominate), then the injection of phase difference from variations in the strip modulus, as counteracted by the structural damping, would be insufficient to change the phase difference trend between the upper and lower work rolls. After sufficient speed increase, however, the net effect of roll-bite parameter variation is to inject overall negative damping, at which point this dominates the structural damping; indeed, even if this speed were less than the critical speed, the work rolls would still go 180 deg out-of-phase. This phenomenon is clearly shown in Fig. 10, where the amplitudes of vibration of the work rolls (WRs) are becoming smaller at first, but as mentioned earlier with this condition, the amount of structural damping also goes down. Once the energies from the negative damping and positive damping become comparable, we see the onset of injection of phase difference from negative damping, and once the energy balance is reached, the roll movements are completely anti-phase and the vibration amplitudes are sustained from there on. In other words, a marginally stable case is a limit of stability in terms of energy. Energy removed by positive damping of the roll-bite model plus positive structural damping combines to equal the energy added to the system by negative damping of the roll-bite model due to certain phase differences in the variation of the roll-bite parameters. Here, even in the marginally stable case, even though the variation in the roll gap is

maintained, the actual amplitudes of vibration of the work rolls decrease because of the structural damping, and once the negative roll-bite damping and positive structural damping energies are equal, we see the system sustain the amplitude of vibration from that point onwards. Therefore, even though the amplitude of vibration reduces for the work rolls, the energy added by the phase difference from the roll-bite parameters maintains the roll gap variation at the same amplitude (or level). This may at first be counterintuitive since, with a decrease in the amplitude of the displacement of the work rolls, the roll gap variation amplitude might initially be thought to decrease. In a truly stable system, however, the rolls will always tend toward in-phase (reaching toward steady-state). But in this marginally stable case, the rolls are vibrating out-of-phase due to the interaction between the roll-bite model and structural model; energy is being added in such a way that the work rolls are kept out of phase. Had the structural damping been lower, however, we would have seen the system go into chatter. But, note that in a "truly" stable system, even absent any structural damping, the system could still be stable due to net positive damping effects from the roll-bite model, i.e., wherein positive damping in the roll-bite model dominates its negative damping. A point to be noted in this discussion is that the specific behavior depends on the amplitude and nature of the disturbance or vibration. If the disturbance is sufficiently large, in the absence of structural damping, many frequencies will manifest in the vibrations of the rolls. This can lead to an unstable or marginally stable system where amplitudes are not required to be the same in each cycle but can be constructively or destructively superimposed with other frequencies.

3D Plots for the upper half surface of the exit thickness profile, and the reduction deviation in exit thickness, are shown in Figs. 11(*a*) and 11(*b*), respectively. Note that reduction deviation (which strongly correlates to the onset of flatness/buckling defects) is defined as the deviation in the thickness strain magnitude at any transverse location x along the strip width relative to the average strip thickness strain magnitude of the strip. Also note that these surface plots represent values relative to the initial steady-state condition prior to coupling the roll-bite model; i.e., the results for time $t > 250$ ms are shown after subtracting corresponding values at $t = 250$ ms.

Interestingly, while the high-frequency variation for the reduction deviation in Fig. 11 represents corresponding thickness deviations, buckling defects may also result due to the low-order variations visible. The plotted lines in Fig. 11 (horizontal lines parallel to the roll axis) have spacing corresponding to the 80-Hz frequency (the roll gap vibration frequency), and therefore, points on the plot where lines on the peaks are visible represent purely 80-Hz vibration, whereas locations where the lines are hidden reveal vibrations at other than 80 Hz. Even though this is a marginally stable system, there is in fact no single frequency of vibration, which is why we see waves of a lower frequency that can manifest in buckle formation. 3D Plots showing the time history of the true mode shapes of the rolls for the marginally stable case are given in Appendix Figs. 20 and 21.

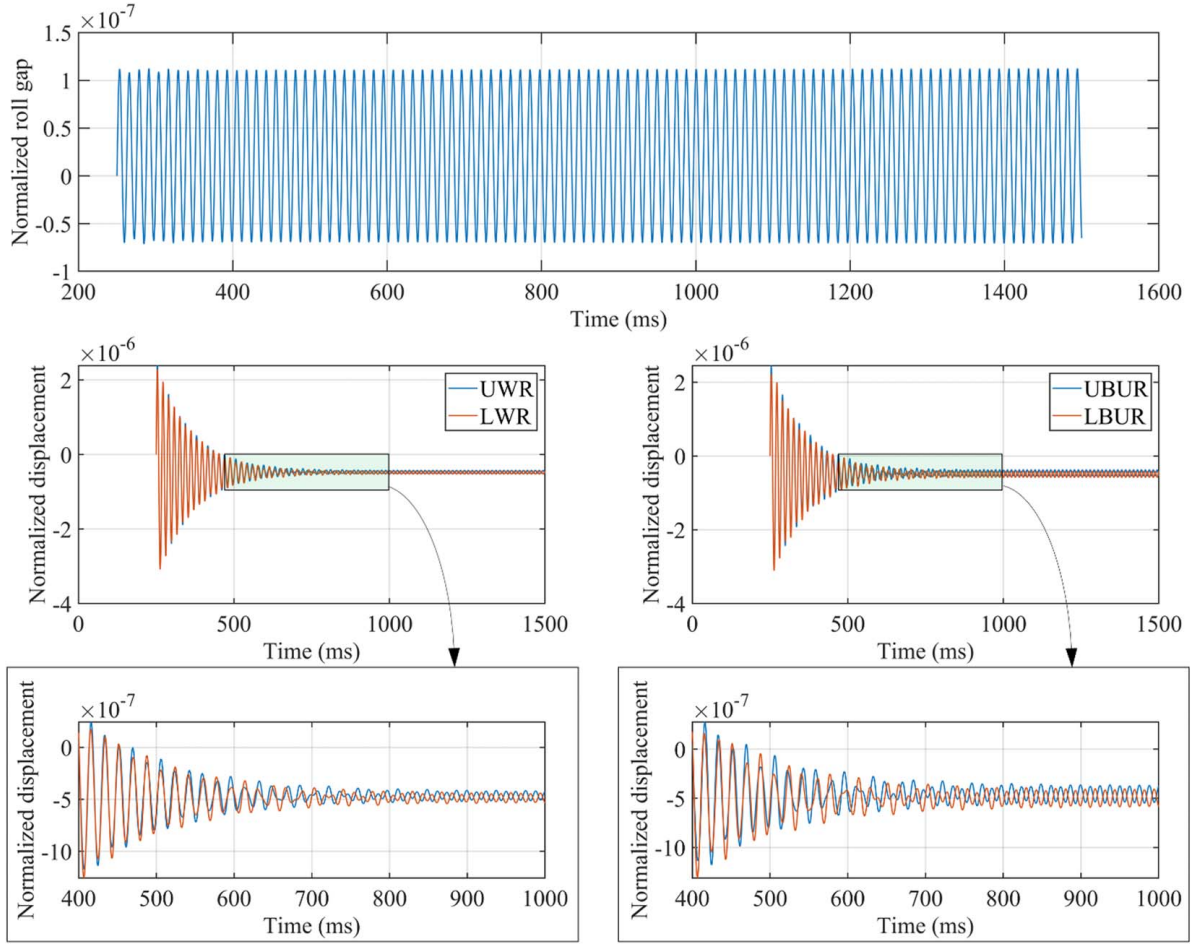

Fig. 10 Time history of (top) normalized roll gap at the axis center; (bottom left) normalized displacement of upper and lower work roll mid-points, and (bottom right) normalized displacement of upper and lower back-up roll mid-points for marginally stable case ($v_r = 8.84$ m/s) with symmetric housing stiffness. Because of the interactions between roll-bite parameter variations and the structural model, a phase difference evolves between the upper and lower roll-stack portions of the mill

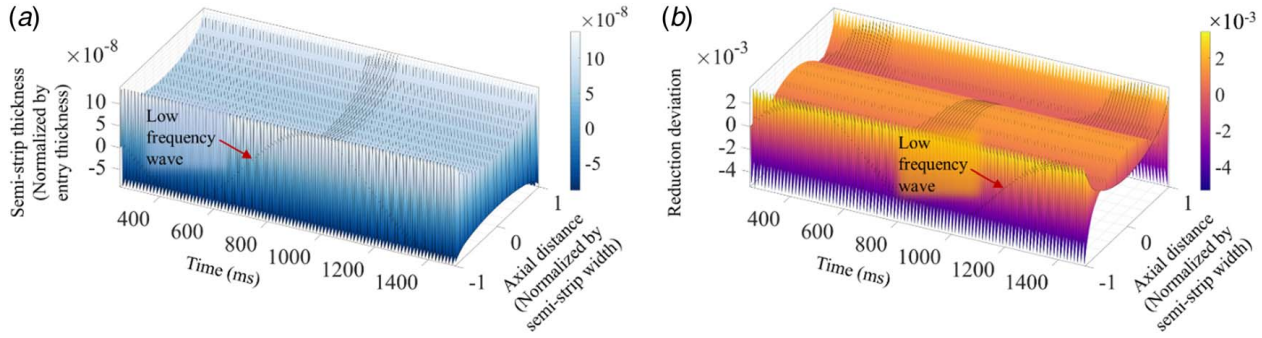

Fig. 11 Time history of exit strip parameters with symmetric housing stiffness for marginally stable case ($v_r = 8.84$ m/s): (*a*) semi-thickness (top half) and (*b*) reduction deviation (used to assess and control flatness). Note: The primary frequency of this variation is 80 Hz, and the frequency of the plotted axial line is also 80 Hz. Coupling of superposition of more than one frequency is clearly visible (shown as low-frequency wave).

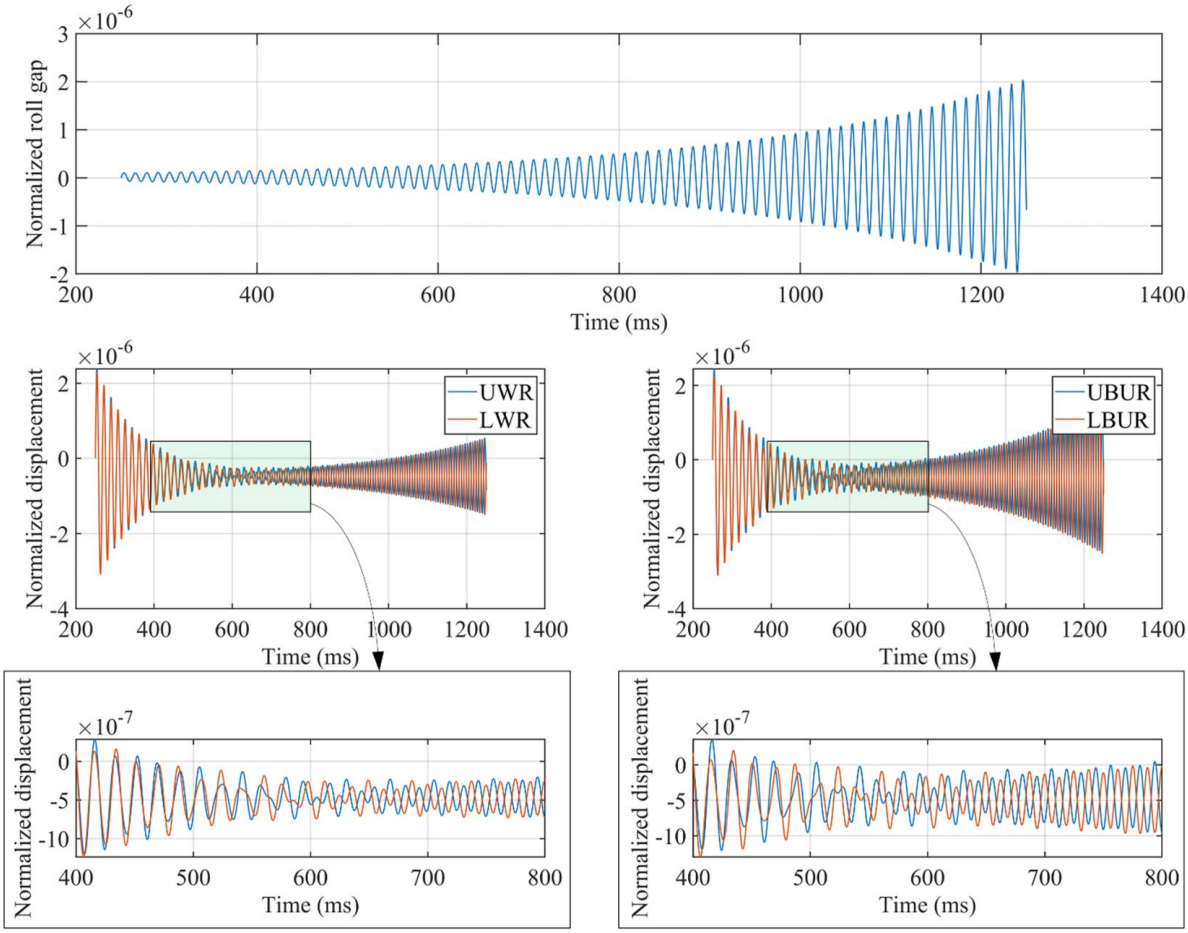

Fig. 12 Time history of (top) normalized roll gap at the axis center; (bottom left) normalized displacement of upper and lower work roll mid-points, and (bottom right) normalized displacement of upper and lower back-up roll mid-points for unstable case ($v_r = 12.7$ m/s) with symmetric housing stiffness

Unstable Case. Increasing the speed beyond the marginally stable speed of 8.84 m/s, transition into an unstable condition occurs. Figure 12 shows results of the roll gap variation and upper and lower stack roll axes displacements relative to the initial steady-state for 12.7 m/s rolling speed.

Here, the fully self-excited vibration (chatter) due to negative damping can be clearly seen. To understand the negative damping phenomenon better, Fig. 13(*a*) provides a comparison of the phase relationships between the roll-bite parameters and roll gap variation for the stable and unstable cases. If one looks particularly at the phase relationship between the roll gap variation and force variation for the unstable case in Fig. 13(*a*), note that the force variation leads roll displacements by about 158.4 deg. This is a different phase relationship than the one proposed by Tlusty et al. [5], wherein it was stated that the phase difference will be 90 deg during chatter due to negative damping. However, the results here agree with the arguments made by Zhao [1] in that the energy added to the system, i.e., to assist the roll movements further by

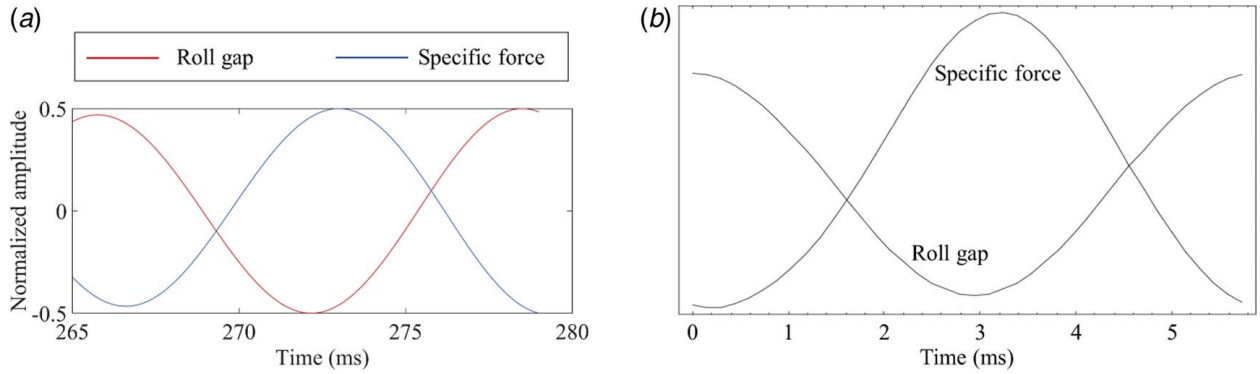

Fig. 13 (*a*) Plot illustrating the phase relationship between the variation in the roll gap and variation in specific rolling force. Note that the specific force is found to lead the roll gap variation by 158.4 deg, which agrees with the phase relationship obtained in Zhao [1], shown in (*b*)

the negative damping, is only due to part of the force, not the entire portion of the force (which would be the case had the phase difference been 90 deg). Note that a one-to-one comparison to Zhao's results in Fig. 13(*b*) [1] is not possible, however, since Zhao used a linear lumped parameter system with different roll-bite process parameters. Nonetheless, the argument that only a part of force contributes to the negative damping can also be clearly seen in the roll displacements (Fig. 12, or even the marginally stable case of Fig. 10).

Thus, whether the onset of chatter occurs or not, this illustrates the fact that only part of the energy is added and used to assist the motions of the rolls since in the initial times (250 ms to 600 ms) the absolute amplitude of vibration of works rolls (and back-up rolls) is decreasing (even though in the unstable case the roll gap is increasing). Note again, however, that the results here do not allow for direct comparison with either Tlusty's or Zhao's. For a more detailed investigation and accurate phase relationship assertions, actual industrial data for the mill and rolling parameters would be required, including the mill housing stiffness. 3D Plots showing the time history of the true mode shapes of the rolls for the unstable case are given in Appendix Figs. 22 and 23.

4-High Mill With Asymmetric Housing Stiffness. Although the foregoing cases represent analogous studies to the vertical symmetry cases typically examined in the literature and involving linear lumped parameter systems, in reality the housing stiffness values at the upper and lower roll-stack supports are different, and indeed, the respective vibrations of rolls in the portions of the upper and lower stack are also asymmetric, as shown in previous work by the authors [27], and experimentally confirmed in Ref. [34]. Accordingly, the symmetric unstable case just examined (12.7 m/s rolling speed) is now simulated using three different lower housing support stiffnesses (double or "2X," quintuple or "5X," and infinite stiffness) applied between the bearing locations on the bottom back-up roll and the bottom of the mill. Figure 14 shows the roll gap variations for these asymmetric housing stiffness cases. It is clearly visible here that, with all three housing stiffness increases at the bottom of the mill, the system becomes stable. Note that the roll gap variations are now no longer converging to the same value. This is because, as alluded to earlier, the initial conditions at the point of roll-bite model coupling (at 250 ms) are unique for each bottom housing stiffness, and once the coupling is enacted, the system stability is governed by the combined effect of energy added or removed through the net negative/positive damping induced via roll-bite variations as well as the energy removed through positive structural damping. 3D Plots showing the time history true mode shapes of the rolls for the cases in this section are given in Appendix B.

Cases With External Disturbance. In the cases discussed until this point, no external disturbance was given; only the natural, residual vibration of very small amplitude remained after an initial mill loading was present at the instant of the roll-bite model coupling with the mill structural model. Although it is widely accepted and experimentally shown that truly self-excited vibration, as in third-octave chatter, does not depend on the nature or amplitude of any disturbance (but rather on the negative

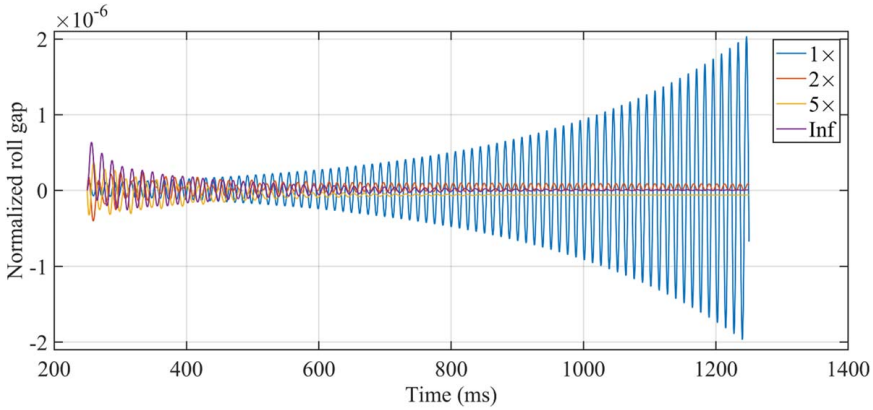

Fig. 14 Time history of the normalized roll gap at the axis center with varying lower housing stiffness for unstable case ($v_r = 12.7$ m/s)

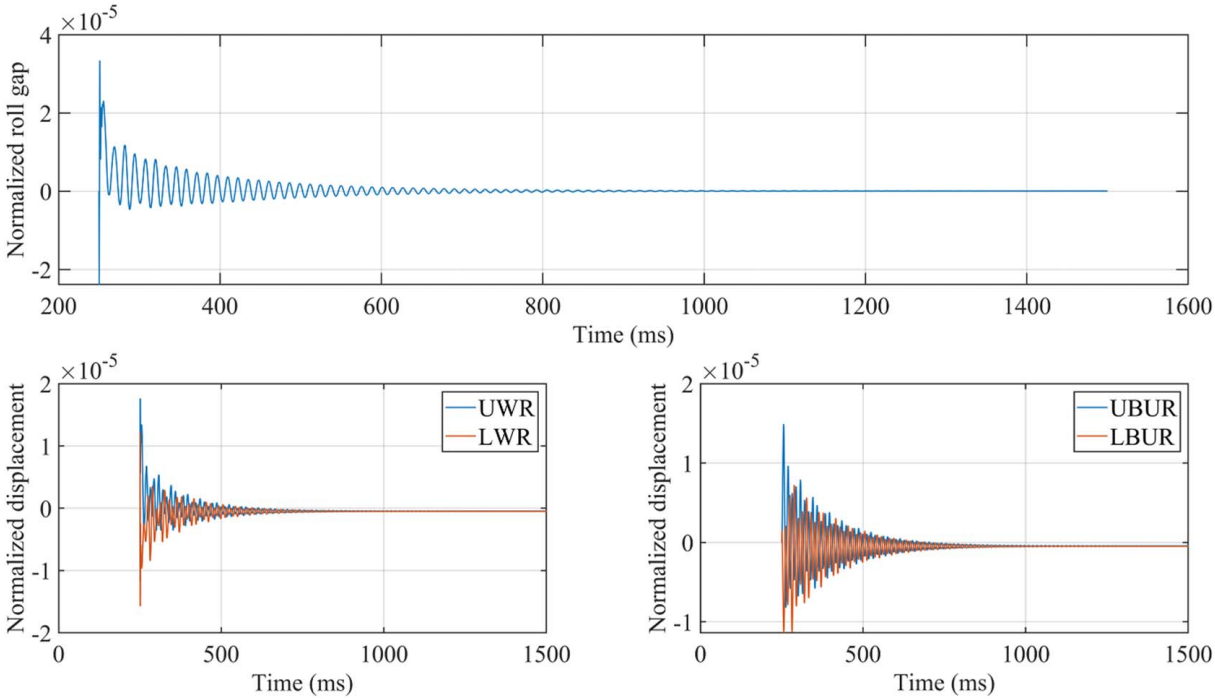

Fig. 15 Time history of (top) normalized roll gap at the axis center; (bottom left) normalized displacement of upper and lower work roll mid-points, and (bottom right) normalized displacement of upper and lower back-up roll mid-points for stable case ($v_r = 5.08$ m/s) with symmetric housing stiffness with impulse disturbance by 1% step change in incoming thickness for 50 μs

damping effect generated due to the phase relationships among variations in the roll-bite parameters and their corresponding interactions with the structural model), to demonstrate the presented model's agreement in this regard the three cases (stable, marginally stable, and unstable) from the first section are now simulated with an impulse disturbance. A 1% step change in the incoming thickness is imposed for the duration of one time-step (5×10^{-5} s) in the NM-Beta transient solution to generate this external impulse disturbance. Figures 15–17 show the respective roll gap variations for the previously indicated stable speed ($v_r = 5.08$ m/s), marginally

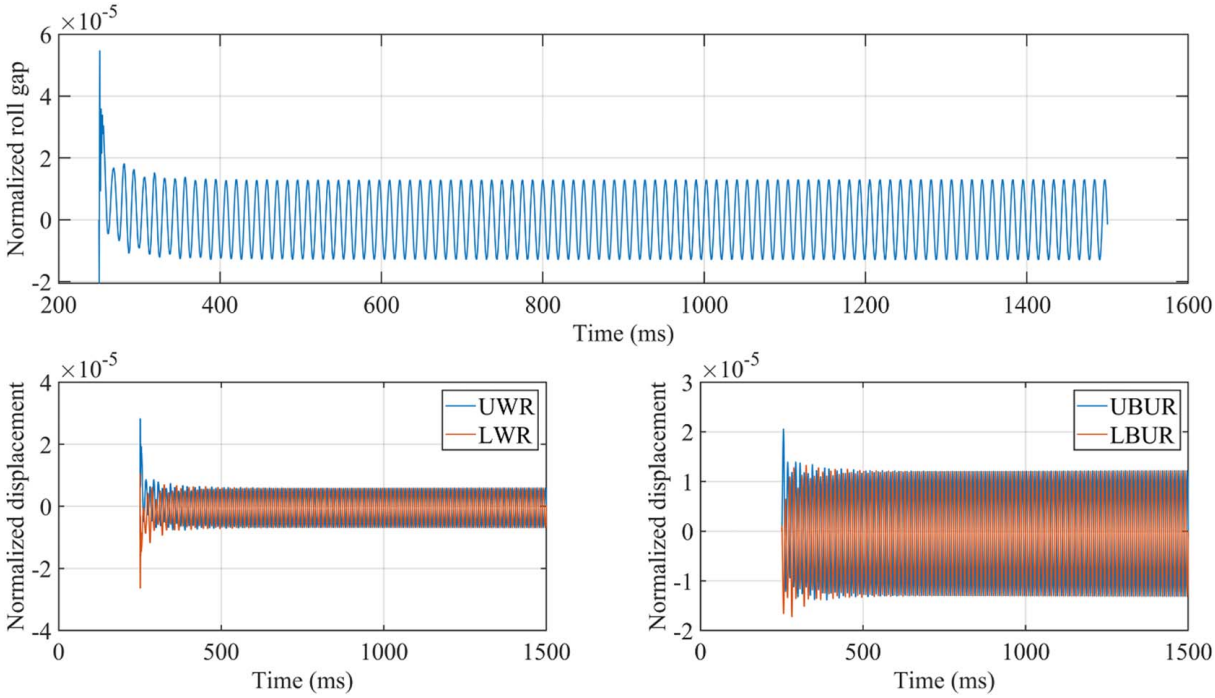

Fig. 16 Time history of (top) normalized roll gap at the axis center; (bottom left) normalized displacement of upper and lower work roll mid-points, and (bottom right) normalized displacement of upper and lower back-up roll mid-points for marginally stable case ($v_r = 8.84$ m/s) with symmetric housing stiffness and impulse disturbance by 1% step change in incoming thickness for 50 μs

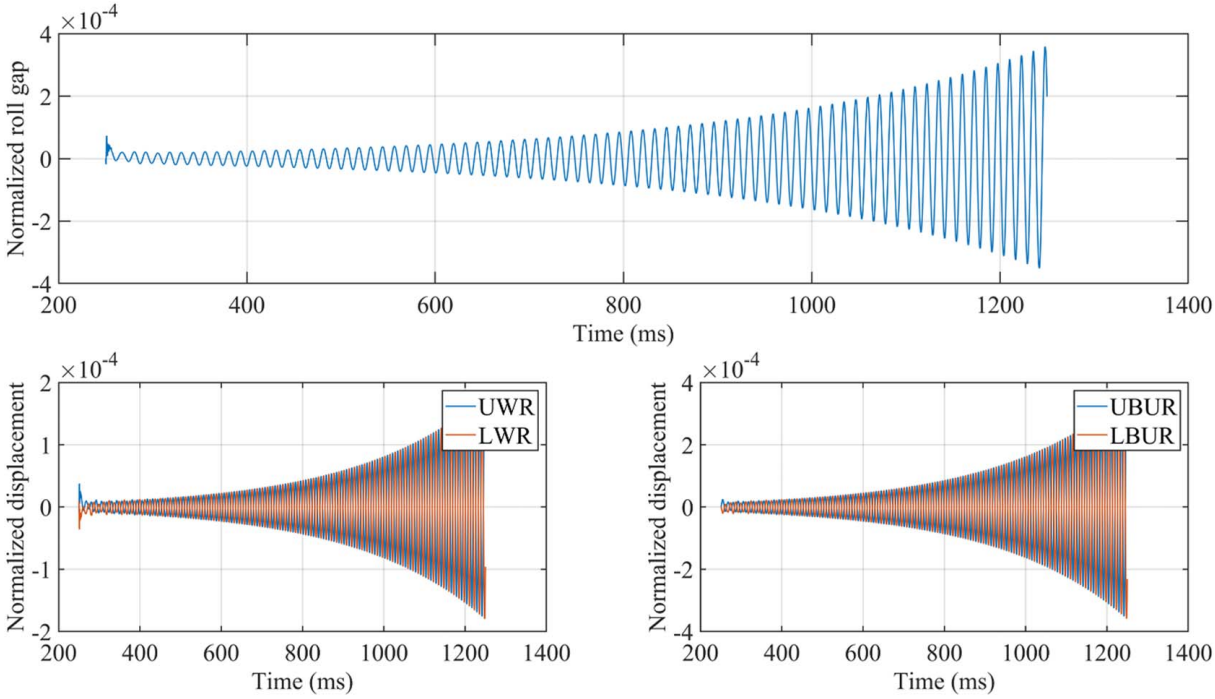

Fig. 17 Time history of (top) normalized roll gap at the axis center; (bottom left) normalized displacement of upper and lower work roll mid-points, and (bottom right) normalized displacement of upper and lower back-up roll mid-points for unstable case (v_r, 12.7 m/s) with symmetric housing stiffness and impulse disturbance by 1% step change in incoming thickness for 50 μs

stable speed ($v_r = 8.84$ m/s), and unstable speed ($v_r = 12.7$ m/s). From the figures, it is clear that with the external disturbance, the absolute values of the variations in the roll-bite model are larger as compared to the disturbance-free cases presented earlier; yet, the overall trends in the system stability (or lack thereof) remain unchanged, as expected. Note that for the stable case, even though a large number of frequencies are excited by the external impulse because the coupled system is inherently stable the structural damping is able to suppress all the frequencies very efficiently. Whereas in marginally stable case, the chatter frequency is not fully suppressed and the vibration is sustained due to energy added by the negative damping effect exciting the chatter frequency. As before, in the unstable case, this negative damping dominates the positive structural damping. It is important to note here that, because the absolute values of variations in the roll-bite model are greater, the amplitudes of vibration for which energy addition and removal is combined are also greater. 3D Plots showing the time history of true mode shapes of the rolls for all the cases are given in Appendix C.

Conclusions

An efficient 3D nonlinear chatter vibration model for cold rolling mills is developed by coupling the mill structural dynamics, obtained via the simplified-mixed finite element method, with a rolling process (roll-bite mechanics) model. Case studies demonstrating the ability of the new model to predict 3D deformation behaviors at the onset of dynamic instability, including for self-excited, third-octave chatter vibration, are presented using a 4-high cold rolling mill. The work, which addresses the lack of available 3D rolling mill chatter studies in the published literature, leads to several key findings:

- The inclusion of 3D bulk-body deformation effects of the rolls, such as coupling between the bending and shear displacements with Hertzian contact flattening, reveals new transverse deformation characteristics under conditions of dynamic instability, including the presence of multi-frequency effects to the strip thickness profile.
- The coupling interactions between the rolling process mechanics and the 3D mill structural dynamics induce phase changes in the motions of the rolls as the stability limit is reached based on increased rolling speed. The results reveal interesting phase relationships not elucidated in previous research, as well as detailed effects from the 3D modeling on the strip profile and shape/flatness.
- Increased dynamic stability and mitigation of chatter are observed via 3D mill deformation time histories when more realistic asymmetry conditions between the upper and lower mill housing stiffness are considered; such effects are not revealed in prior studies that adopt vertical symmetry.
- In contrast to the prior, linear lumped parameter model representations, the nonlinear 3D chatter vibration model reveals more complex, multi-frequency vibration modes within the roll-stack, which lead to corresponding multi-frequency defects on the rolled strip thickness profile.

Acknowledgment

The authors gratefully acknowledge support for this work from the National Science Foundation (Grant No. CMMI-1555531).

Conflict of Interest

There are no conflicts of interest.

Data Availability Statement

The data sets generated and supporting the findings of this article are obtainable from the corresponding author upon reasonable request.

Appendix A

Figures 18–23

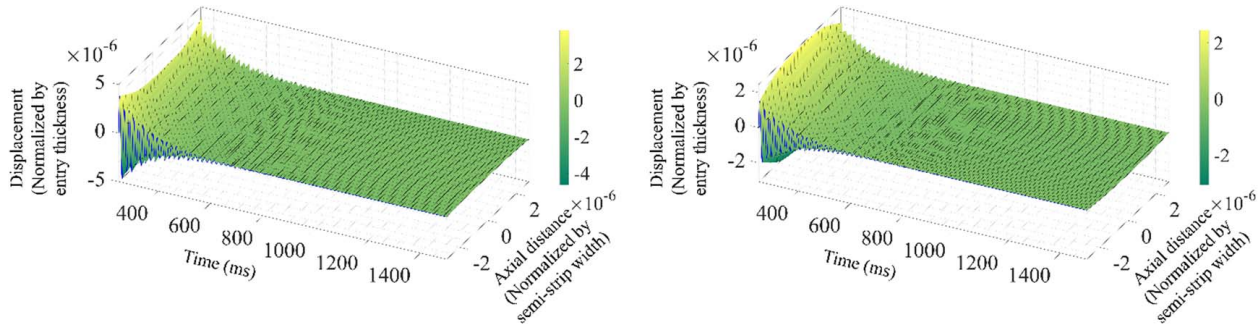

Fig. 18 Time history of normalized displacement with symmetric housing stiffness: (left) upper work roll axis displacement, and (right) upper back-up roll axis displacement, relative to the assumed steady-state (250 ms) for stable case ($v_r = 5.08$ m/s)

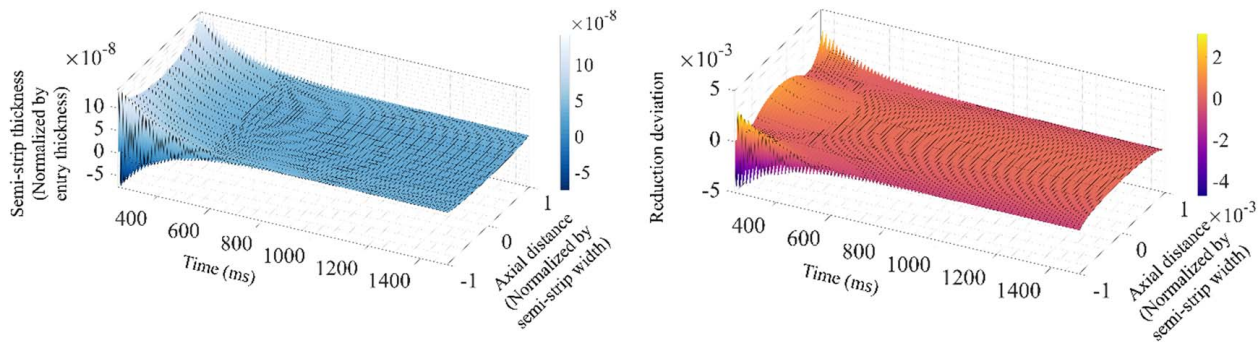

Fig. 19 Time history of exit strip parameters with symmetric housing stiffness: (left) semi-thickness (top surface), and (right) reduction deviation, relative to the assumed steady-state (250 ms) for the stable case ($v_r = 5.08$ m/s)

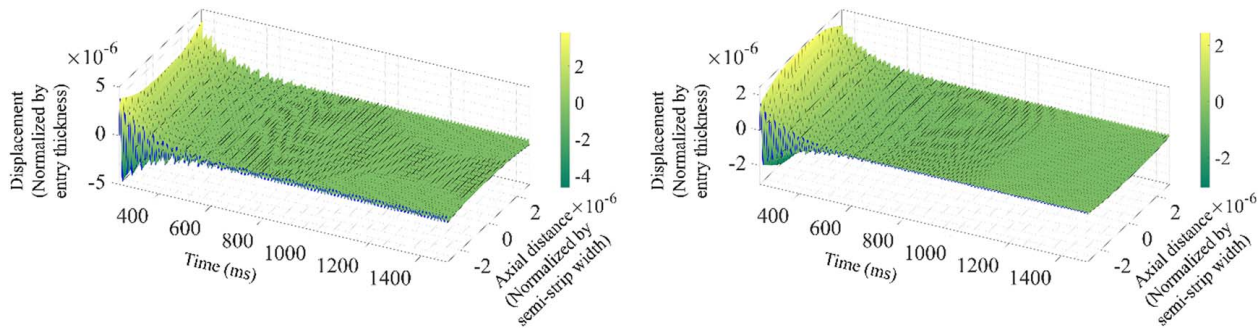

Fig. 20 Time history of normalized displacement with symmetric housing stiffness: (left) upper work roll axis displacement, and (right) upper back-up roll axis displacement, relative to the assumed steady-state (250 ms) for marginally stable case ($v_r = 8.84$ m/s)

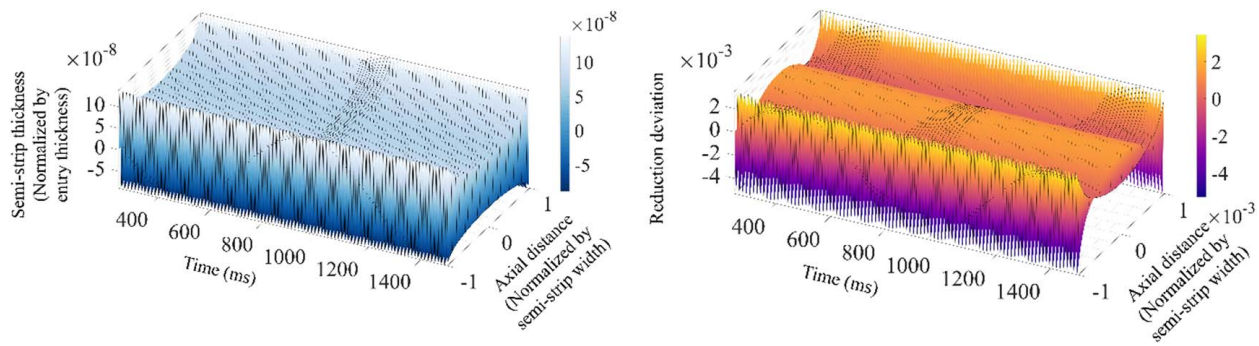

Fig. 21 Time history of exit strip parameters with symmetric housing stiffness: (left) semi-thickness (top surface), and (right) reduction deviation, relative to the assumed steady-state (250 ms) for the marginally stable case ($v_r = 8.84$ m/s)

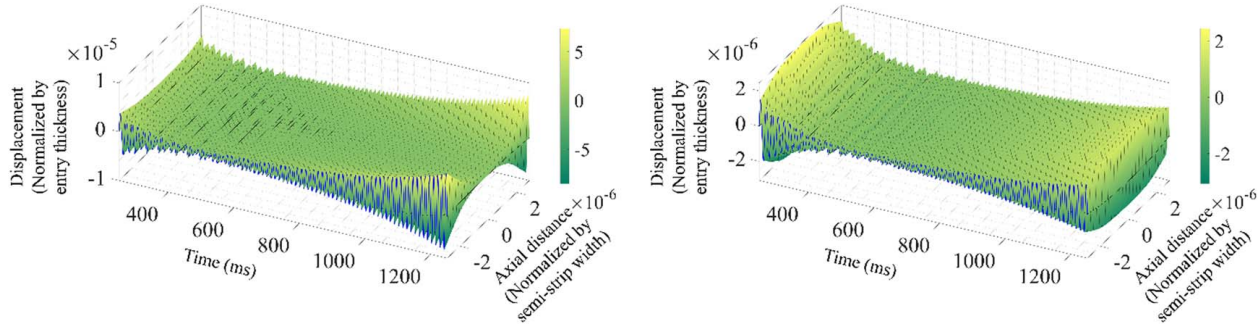

Fig. 22 Time history of normalized displacement with symmetric housing stiffness: (left) upper work roll axis displacement, and (right) upper back-up roll axis displacement, relative to the assumed steady-state (250 ms) for unstable case ($v_r = 12.7$ m/s)

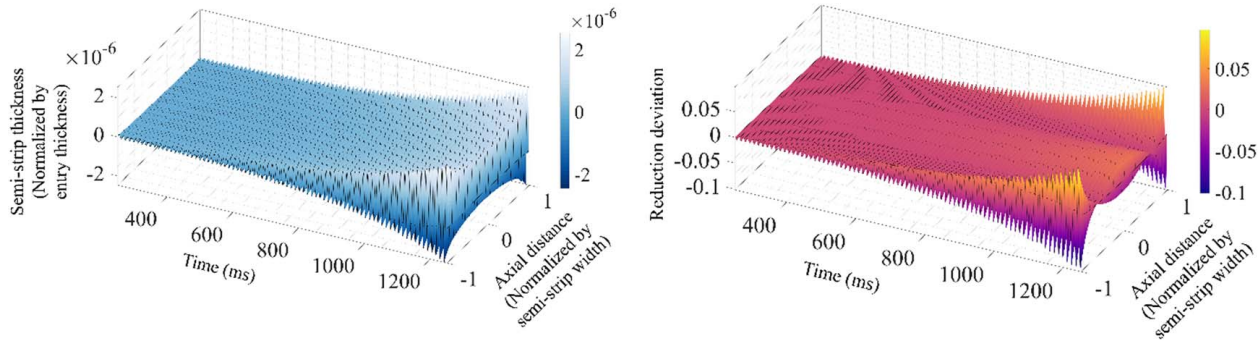

Fig. 23 Time history of exit strip parameters with symmetric housing stiffness: (left) semi-thickness (top surface), and (right) reduction deviation, relative to the assumed steady-state (250 ms) for unstable case ($v_r = 12.7$ m/s)

Appendix B

Figures 24–29

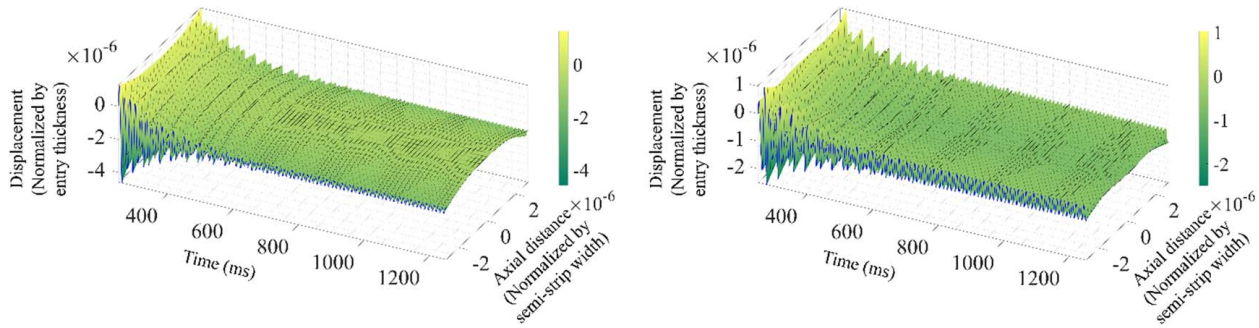

Fig. 24 Time history of normalized displacement with 2 × (double) lower housing stiffness: (left) upper work roll axis displacement, and (right) lower work roll axis displacement, relative to the assumed steady-state (250 ms) for unstable case ($v_r = 12.7$m/s)

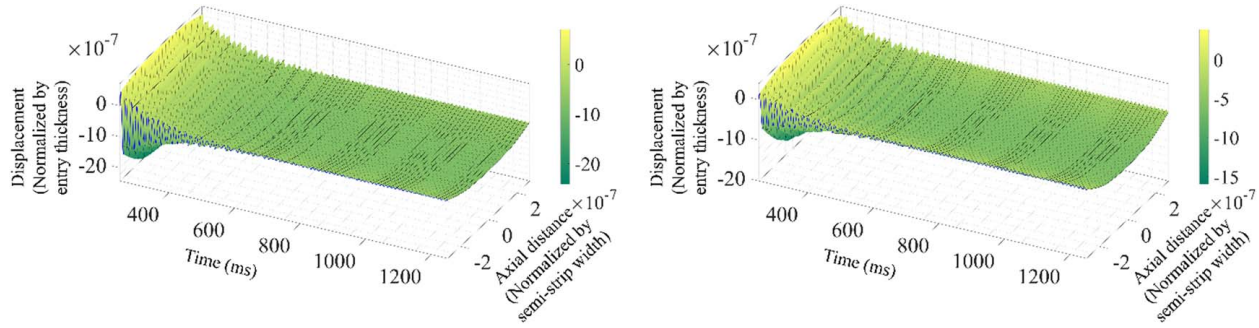

Fig. 25 Time history of normalized displacement with 2 × (double) lower housing stiffness: (left) upper back-up roll axis displacement, and (right) lower back-p oll axis displacement, relative to the assumed steady-state (250 ms) for unstable case ($v_r = 12.7$ m/s)

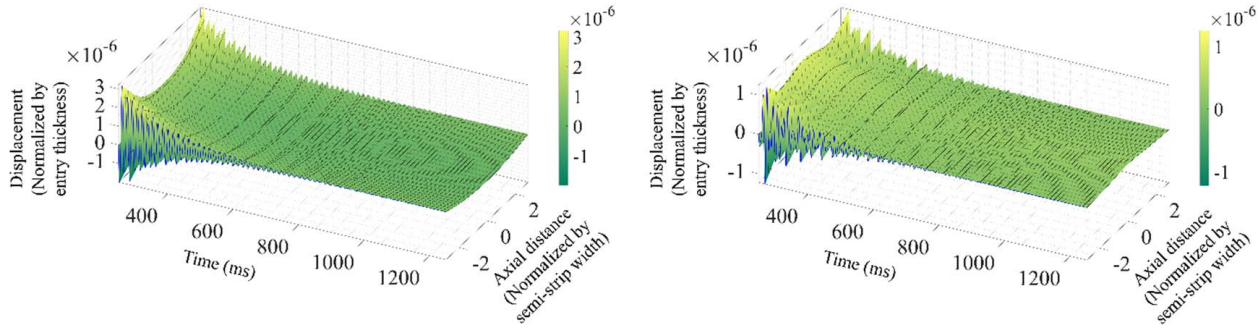

Fig. 26 Time history of normalized displacement with 5× (quintuple) lower housing stiffness: (left) upper work roll axis displacement, and (right) lower work roll axis displacement, relative to the assumed steady-state (250 ms) for unstable case ($v_r = 12.7$m/s)

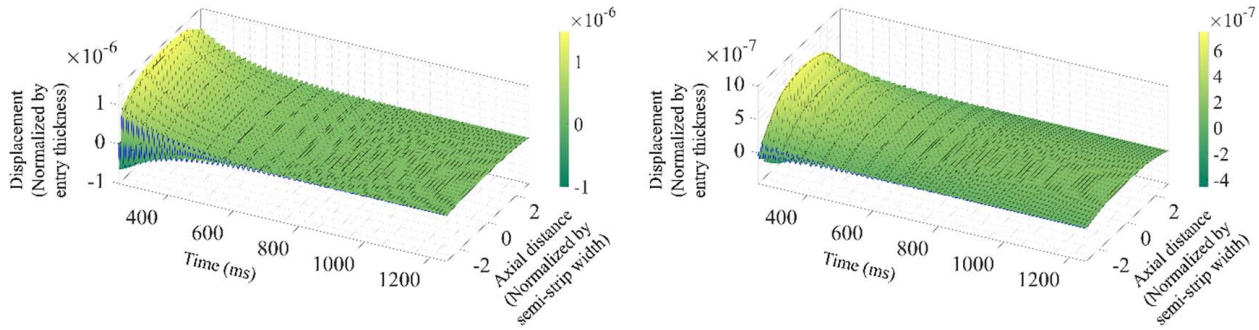

Fig. 27 Time history of normalized displacement with 5× (quintuple) lower housing stiffness: (left) upper back-up roll axis displacement, and (right) lower back-up roll axis displacement, relative to the assumed steady-state (250 ms) for unstable case ($v_r = 12.7$ m/s)

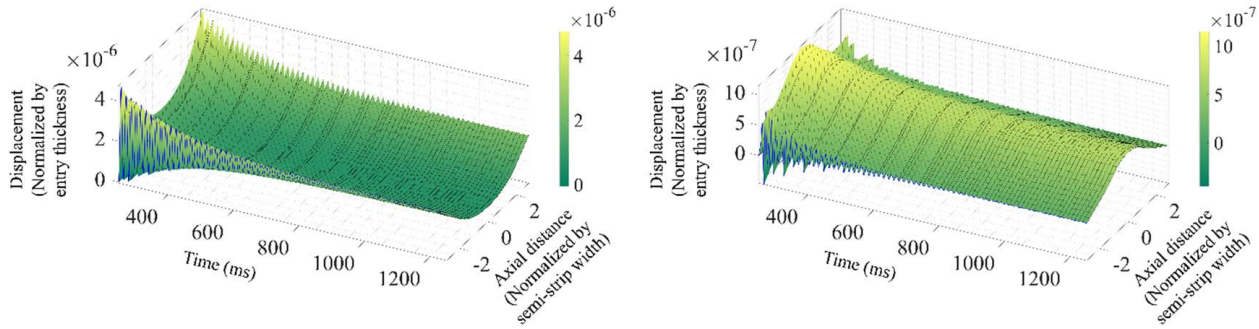

Fig. 28 Time history of normalized displacement with "infinite" lower housing stiffness: (left) upper work roll axis displacement, and (right) lower work roll axis displacement, relative to the assumed steady-state (250 ms) for unstable case ($v_r = 12.7$ m/s)

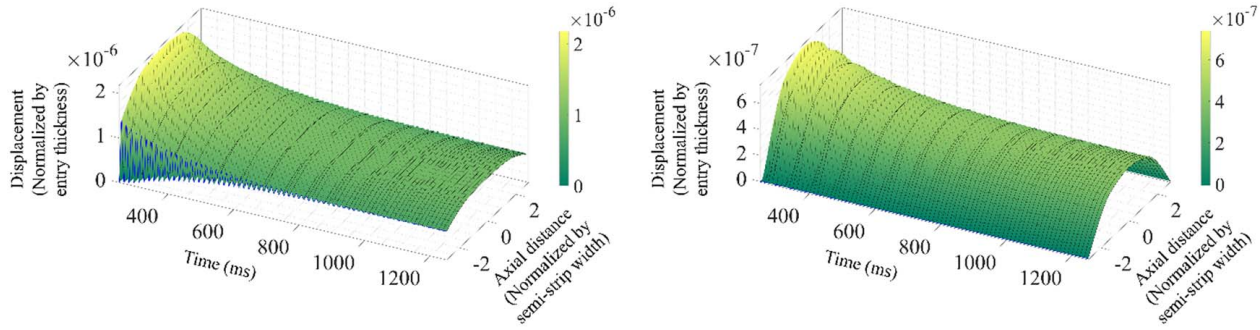

Fig. 29 Time history of normalized displacement with "infinite" lower housing stiffness: (left) upper back-up roll axis displacement, and (right) lower back-up roll axis displacement, relative to the assumed steady-state (250 ms) for unstable case ($v_r = 12.7$ m/s)

Appendix C

Figures 30–32

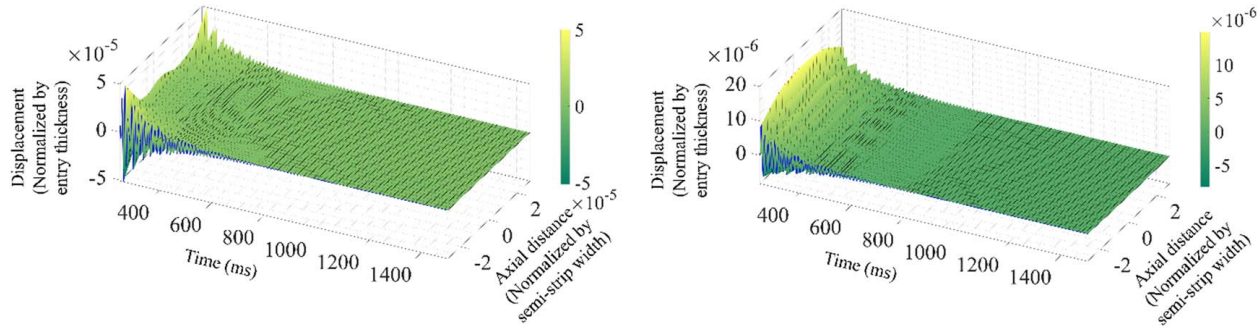

Fig. 30 Time history of normalized displacement with symmetric housing stiffness and external impulse disturbance: (left) upper work roll axis displacement, and (right) upper back-up roll axis displacement, relative to the assumed steady-state (250 ms) for stable case ($v_r = 5.08$ m/s). Note that time history is shown one time-step after the disturbance, i.e., from 250.1 ms.

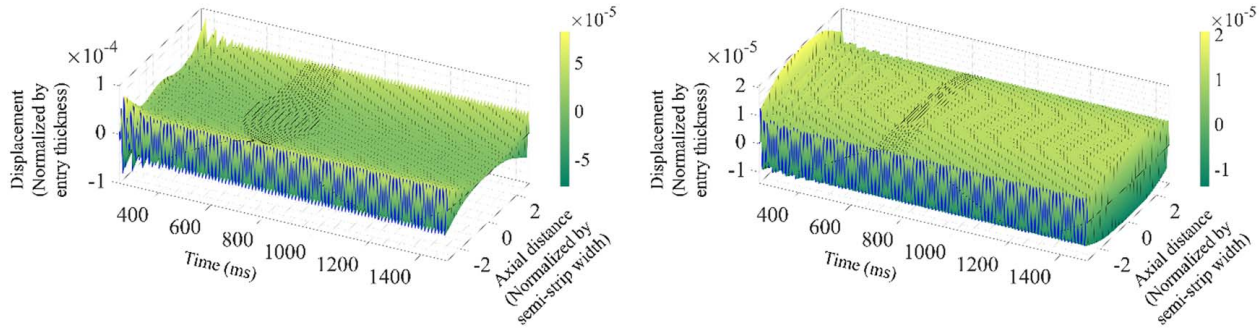

Fig. 31 Time history of normalized displacement with symmetric housing stiffness and external impulse disturbance: (left) upper work roll axis displacement, and (right) upper back-up roll axis displacement, relative to the assumed steady-state (250 ms) for marginally stable case ($v_r = 8.84$ m/s). Note that time history is shown one time-step after the disturbance, i.e., from 250.1 ms.

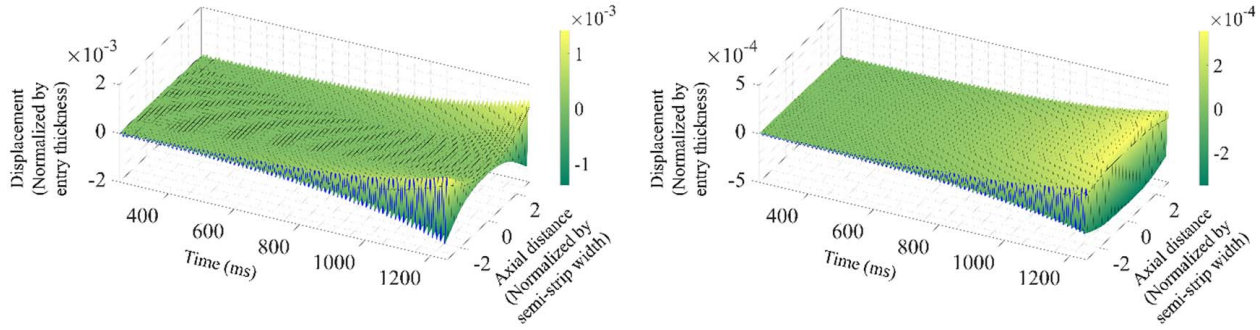

Fig. 32 Time history of normalized displacement with symmetric housing stiffness and external impulse disturbance: (left) upper work roll axis displacement, and (right) upper back-up roll axis displacement, relative to the assumed steady-state (250 ms) for unstable case ($v_r = 12.7$ m/s). Note that time history is shown one time-step after the disturbance, i.e., from 250.1 ms.

References

[1] Zhao, H., 2008, "Regenerative Chatter in Cold Rolling," Ph.D. dissertation, Northwestern University, Evanston, IL.

[2] 2016, "Roll and Strip Chatter Marks; 5th Octave Chatter," Innoval Technol. https://www.innovaltec.com/strip-chatter-marks-blog/, Accessed 26 March 2022.

[3] Yun, I. S., Wilson, W. R. D., and Ehmann, K. F., 1998, "Review of Chatter Studies in Cold Rolling," Int. J. Mach. Tools Manuf., **38**(12), pp. 1499–1530.

[4] Hu, P.-H., 1998, "Stability and Chatter in Rolling," Ph.D., Northwestern University, Evanston, IL.

[5] Tlusty, J., Chandra, G., Critchley, S., and Paton, D., 1982, "Chatter in Cold Rolling," CIRP Ann., **31**(1), pp. 195–199.

[6] Yun, I.-S., Wilson, W. R. D., and Ehmann, K. F., 1998, "Chatter in the Strip Rolling Process, Part 1: Dynamic Model of Rolling," ASME J. Manuf. Sci. Eng., **120**(2), pp. 330–336.

[7] Tamiya, T., Furui, K., and Iida, H., 1980, "Analysis of Chattering Phenomenon in Cold Rolling," Proceedings of the International Conference on Steel Rolling, Tokyo, Japan, Sept. 29–Oct. 4, pp. 1191–1202.

[8] Yun, I.-S., Ehmann, K. F., and Wilson, W. R. D., 1998, "Chatter in the Strip Rolling Process, Part 2: Dynamic Rolling Experiments," ASME J. Manuf. Sci. Eng., **120**(2), pp. 337–342.

[9] Yun, I.-S., Ehmann, K. F., and Wilson, W. R. D., 1998, "Chatter in the Strip Rolling Process, Part 3: Chatter Model," ASME J. Manuf. Sci. Eng., **120**(2), pp. 343–348.
[10] Wanheim, T., and Bay, N., 1978, "A Model for Friction in Metal Forming Processes," CIRP Ann. Manuf. Technol., **27**, pp. 189–194.
[11] Bland, D. R., and Ford, H., 1948, "The Calculation of Roll Force and Torque in Cold Strip Rolling With Tensions," Proc. Inst. Mech. Eng., **159**(1), pp. 144–163.
[12] Yarita, I., Furukawa, K., Seino, Y., Takimoto, T., Nakazato, Y., and Nakagawa, K., 1978, "An Analysis of Chattering in Cold Rolling for Ultrathin Gauge Steel Strip," Trans. Iron Steel Inst. Jpn., **18**(1), pp. 1–10.
[13] Chefneux, L., Fischbach, J.-P., and Gouzou, J., 1984, "Study and Industrial Control of Chatter in Cold Rolling," Iron Steel Eng., **61**(11), pp. 17–26.
[14] Lin, Y.-J., Suh, C. S., Langari, R., and Noah, S. T., 2003, "On the Characteristics and Mechanism of Rolling Instability and Chatter," ASME J. Manuf. Sci. Eng., **125**(4), pp. 778–786.
[15] Kimura, Y., Sodani, Y., Nishiura, N., Ikeuchi, N., and Mihara, Y., 2003, "Analysis of Chatter in Tandem Cold Rolling Mills," ISIJ Int., **43**(1), pp. 77–84.
[16] Kapil, S., Eberhard, P., and Dwivedy, S. K., 2014, "Nonlinear Dynamic Analysis of a Parametrically Excited Cold Rolling Mill," ASME J. Manuf. Sci. Eng., **136**(4), p. 041012.
[17] Hu, P.-H., and Ehmann, K. F., 2000, "A Dynamic Model of the Rolling Process. Part I: Homogeneous Model," Int. J. Mach. Tools Manuf., **40**(1), pp. 1–19.
[18] Hu, P.-H., and Ehmann, K. F., 2000, "A Dynamic Model of the Rolling Process. Part II: Inhomogeneous Model," Int. J. Mach. Tools Manuf., **40**(1), pp. 21–31.
[19] Kim, Y., Kim, C.-W., Lee, S.-J., and Park, H., 2012, "Experimental and Numerical Investigation of the Vibration Characteristics in a Cold Rolling Mill Using Multibody Dynamics," ISIJ Int., **52**(11), pp. 2042–2047.
[20] Mehrabi, R., Salimi, M., and Ziaei-Rad, S., 2015, "Finite Element Analysis on Chattering in Cold Rolling and Comparison With Experimental Results," ASME J. Manuf. Sci. Eng., **137**(6), p. 061013.
[21] Niroomand, M. R., Forouzan, M. R., and Salimi, M., 2015, "Theoretical and Experimental Analysis of Chatter in Tandem Cold Rolling Mills Based on Wave Propagation Theory," ISIJ Int., **55**(3), pp. 637–646.
[22] Brusa, E., Lemma, L., and Benasciutti, D., 2010, "Vibration Analysis of a *Sendzimir* Cold Rolling Mill and Bearing Fault Detection," Proc. Inst. Mech. Eng. Part C J. Mech. Eng. Sci., **224**(8), pp. 1645–1654.
[23] Lu, X., Sun, J., Li, G., Wang, Q., and Zhang, D., 2019, "Dynamic Analysis of Vibration Stability in Tandem Cold Rolling Mill," J. Mater. Process. Technol., **272**, pp. 47–57.
[24] Sun, J., Peng, Y., and Liu, H., 2014, "Dynamic Characteristics of Cold Rolling Mill and Strip Based on Flatness and Thickness Control in Rolling Process," J. Cent. South Univ., **21**(2), pp. 567–576.
[25] Kapil, S., Eberhard, P., and Dwivedy, S. K., 2016, "Dynamic Analysis of Cold-Rolling Process Using the Finite-Element Method," ASME J. Manuf. Sci. Eng., **138**(4), p. 041002.
[26] Brusa, E., and Lemma, L., 2009, "Numerical and Experimental Analysis of the Dynamic Effects in Compact Cluster Mills for Cold Rolling," J. Mater. Process. Technol., **209**(5), pp. 2436–2445.
[27] Patel, A., Malik, A., and Mathews, R., 2022, "Efficient Three-Dimensional Model to Predict Time History of Structural Dynamics in Cold Rolling Mills," ASME J. Manuf. Sci. Eng., **144**(7), p. 071009.
[28] Zhang, F., and Malik, A. S., 2021, "An Efficient Multi-scale Modeling Method That Reveals Coupled Effects Between Surface Roughness and Roll-Stack Deformation in Cold Sheet Rolling," ASME J. Manuf. Sci. Eng., **143**(10), p. 101005.
[29] Malik, A. S., and Grandhi, R. V., 2008, "A Computational Method to Predict Strip Profile in Rolling Mills," J. Mater. Process. Technol., **206**(1–3), pp. 263–274.
[30] Zhang, F., and Malik, A., 2018, "A Roll-Stack Contact Mechanics Model to Predict Strip Profile in Rolling Mills With Asymmetric, Continuously Variable Crown Rolls," ASME J. Manuf. Sci. Eng., **140**(1), p. 011008.
[31] Patel, A., Malik, A. S., Mathews, R., and Zhang, F., 2022, "Influence of Work-Roll Grinding Error and High-Fidelity Corrective Grinding in Cold Sheet Rolling," Int. J. Adv. Manuf. Tech., **120**(11–12), pp. 7389–7413.
[32] Linghu, K., Jiang, Z., Zhao, J., Li, F., Wei, D., Xu, J., Zhang, X., and Zhao, X., 2014, "3D FEM Analysis of Strip Shape During Multi-pass Rolling in a 6-High CVC Cold Rolling Mill," Int. J. Adv. Manuf. Tech., **74**(9–12), pp. 1733–1745.
[33] Zhang, F., Malik, A., and Yu, H., 2018, "High-Fidelity Roll Profile Contact Modeling by Simplified Mixed Finite Element Method," Proceeding of the 2018 ASME Manufacturing Science Engineering Conference (MSEC 2018), College Station, TX, June 18–22, p. V004T03A03.
[34] Paton, D. L., and Critchley, S., 1985, "Tandem Mill Vibration: Its Cause and Control," Proceedings of the 26th Mechanical Working and Steel Processing Conference, Chicago, IL, Iron & Steel Society.